NOVEL MEMBRANE AND DEVICE FOR DIRECT CONTACT MEMBRANE DISTILLATION-BASED DESALINATION PROCESS: PHASE II

New Jersey Institute of Technology
Newark, New Jersey

Agreement No. 01-FC-81-0737

Desalination and Water Purification Research and Development Program Final Report No. 96

July 2003

U.S. Department of the Interior
Bureau of Reclamation
Denver Office
Technical Service Center
Environmental Resources Team
Water Treatment Engineering and Research Group

REPORT DOCUMENTATION PAGE

Form Approved
OMB No. 0704-0188

1. AGENCY USE ONLY *(Leave Blank)*	2. REPORT DATE	3. REPORT TYPE AND DATES COVERED
	July 2003	Final

4. TITLE AND SUBTITLE
NOVEL MEMBRANE AND DEVICE FOR DIRECT CONTACT MEMBRANE DISTILLATION-BASED DESALINATION PROCESS: PHASE II

5. FUNDING NUMBERS
01-FC-81-0737

6. AUTHOR(S)
K.K.Sirkar and Baoan Li

7. PERFORMING ORGANIZATION NAME(S) AND ADDRESS(ES)
New Jersey Institute of Technology
Center for Membrane Technologies
Room 362 Tiernan Hall
323 Dr. King Blvd
Newark, NJ 07102

8. PERFORMING ORGANIZATION REPORT NUMBER

9. SPONSORING/MONITORING AGENCY NAME(S) AND ADDRESS(ES)
Bureau of Reclamation
Denver Federal Center
PO Box 25007
Denver CO 80225-0007

10. SPONSORING/MONITORING AGENCY REPORT NUMBER
DWPR No. 96

11. SUPPLEMENTARY NOTES

12a. DISTRIBUTION/AVAILABILITY STATEMENT
Available from the National Technical Information Service, Operations Division, 5285 Port Royal Road, Springfield, Virginia 22161

12b. DISTRIBUTION CODE

13. ABSTRACT ***(Maximum 200 words)***
Direct contact membrane distillation (DCMD) of brine for desalination suffers from long-term flux decay due to pore wetting, low water flux due to poor transport coefficients in the hot brine, conductive heat loss in thin-wall membranes and considerable temperature rise of the cold distillate. Using different porous hydrophobic polypropylene hollow fiber membranes having different plasmapolymerized coatings of silicone-fluoropolymers on the outside surface, rectangular cross flow modules were developed with hot brine flowing across the outside of the fibers; cold distillate flowed through the fiber bores in DCMD whereas a vacuum was applied in the fiber bores in vacuum membrane distillation (VMD). In a small module built of larger diameter fibers (330μm internal diameter (I.D.)), a DCMD-based water vapor flux as high as 79 kg/m^2-h was achieved with 90 °C brine; brine at 85 °C in VMD yielded a flux of 70 kg/m^2-h. An extended-term (120 hours) DCMD test for the same module with 85 °C brine yielded a steady water flux of 54 kg/m^2-h. These and other results suggest that highly permeable coatings, larger fiber I.D., wall porosity and pore size, appropriate distillate flow rates and higher hot brine cross-flow velocities can lead to a stable and high water vapor flux in DCMD.

14. SUBJECT TERMS - -
membrane distillation, polypropylene hollow fibers, desalination, microporous silicone coating, cross-flow modules

15. NUMBER OF PAGES
90

16. PRICE CODE

17. SECURITY CLASSIFICATION OF REPORT	18. SECURITY CLASSIFICATION OF THIS PAGE	19. SECURITY CLASSIFICATION OF ABSTRACT	20. LIMITATION OF ABSTRACT
UL	UL	UL	UL

NOVEL MEMBRANE AND DEVICE FOR DIRECT CONTACT MEMBRANE DISTILLATION-BASED DESALINATION PROCESS: PHASE II

Dr. Kamalesh K. Sirkar
Dr. Baoan Li
New Jersey Institute of Technology
Newark, New Jersey

Agreement No. 01-FC-81-0737

Desalination and Water Purification Research and Development Program Final Report No. 96

July 2003

U.S. Department of the Interior
Bureau of Reclamation
Denver Office
Technical Service Center
Environmental Resources Team
Water Treatment Engineering and Research Group

MISSION STATEMENTS

U.S. Department of the Interior

The mission of the Department of the Interior is to protect and provide access to our Nation's natural and cultural heritage and honor our trust responsibilities to Indian tribes and our commitments to island communities.

Bureau of Reclamation

The mission of the Bureau of Reclamation is to manage, develop, and protect water and related resources in an environmentally and economically sound manner in the interest of the American public.

Disclaimer

Information contained in this report regarding commercial products or firms was supplied by those firms. It may not be used for advertising or promotional purposes and is not to be construed as an endorsement of any product or firm by the Bureau of Reclamation**.**

The information contained in this report was developed for the Bureau of Reclamation; no warranty as to the accuracy, usefulness, or completeness is expressed or implied.

ACKNOWLEDGMENTS

The research conducted under this contract was sponsored by Desalination and Water Purification Research and Development Program, Bureau of Reclamation, Denver, Colorado. Ms. Yin Wu and Mr. Praveen Kosaraju helped Dr. Baoan Li substantially during the experiments conducted between January and August 2002. Dr. Sudipto Majumdar helped the project during October and November 2001 as well as helping Dr. Baoan Li in developing the entrance sections for all modules and other activities.

Table of Contents

List of Tables

List of Figures

Glossary

A_r	membrane area ratio for heat transfer through a membrane surface
A_{rf}	value of A_r for hot brine-membrane interface, d_o / d_i
$A_{r\ln}$	value of A_r for logarithmic mean membrane area, $d_{r\ln} / d_i$, where logarithmic mean diameter, $d_{r\ln} = (d_o - d_i) / \ln(d_o / d_i)$
A_{rp}	value of A_r for cold distillate- membrane interface, which is equal to 1
cm	centimeter
c_p	liquid heat capacity
C	salt concentration
d	fiber I.D. or O.D.
d_i	fiber inside diameter (I.D.)
d_o	fiber outside diameter (O.D.)
D	characteristic dimension
DCMD	direct contact membrane distillation
D.I.water	deionized water
F	water vapor flux
F_c	tube-row correction factor
h	overall boundary layer heat transfer coefficient
h_c	effective membrane heat transfer coefficient
h_f	shell side boundary layer heat transfer coefficient
h_{mg}	heat transfer coefficient of the vapor/gas within the membrane pores
h_{ms}	heat transfer coefficient of the solid polymeric membrane material
h_m	membrane heat transfer coefficient
h_p	tube side boundary layer heat transfer coefficient
hr	hour
h_v	heat transfer coefficient related to the water vapor flux
Hg	mercury
I.D.	internal diameter
k	liquid thermal conductivity
kg	kilogram
L	fiber length
min	minutes
MD	membrane distillation
n	number of fibers in a membrane module
Nu	Nusselt number
N_V	mass flux of water vapor across the membrane
O.D.	outside diameter
p_{fm}	water vapor partial pressure at hot brine-membrane interface
p_{pm}	water vapor partial pressure at cold distillate-membrane interface
P_1	atmospheric pressure

Pr	Prandtl number
Pr_w	Prandtl number evaluated at the tube-wall temperature
Q	effective heat flux through the membrane
Q_{N_2}	permeability coefficient of N_2 permeation through the membrane of effective thickness δ_M
Q_{N_2}/δ_M	N_2 permeance
Q_m	heat flux conducted through the nonporous solid polymeric part of the membrane and the gas phase that fills the pores
Q_V	heat flux transferred by vapor flux across the membrane
Re	Reynolds Number
Re_d	diameter-based Reynolds number
RO	reverse osmosis
s	inside membrane area ($= n\pi d_i L$)
STP	T_0 = 273.15 K, P_0 = 760 Torr
T	temperature
T_1	room temperature
T_f	bulk temperature of feed
T_{fm}	interface temperature on the surface of membrane in feed side
T_{fm}/T_f	degree of temperature polarization in VMD
TPC	temperature polarization coefficient
U	overall heat transfer coefficient of DCMD process
V	velocity
V_1	volume flow rate of gas through the membrane during measurement at room temperature
V_{feed}	volume flow rate of the feed
VMD	vacuum membrane distillation
ρ	density
ΔP_{N_2}	N_2 pressure difference across the membrane
μ	dynamic viscosity (absolute viscosity)
μ_W	liquid viscosity evaluated at the tube-wall temperature
η	membrane heat transfer efficiency
ΔH_V	heat of vaporization of water
ΔT	bulk temperature difference between feed and distillate ($T_f - T_p$)
ΔT_f	temperature drop of feed along the module length
ΔT_F	temperature difference between brine bulk temperature and the temperature of brine-membrane interface on the feed side
ΔT_m	trans-membrane temperature difference

ΔT_P	the temperature difference between the temperature of membrane-distillate interface and distillate bulk temperature on distillate side
δ_M	effective thickness of membrane
ε	membrane porosity

1. Executive Summary

Although research and development studies to improve commercialized reverse osmosis and thermally-driven desalination processes are continuing, there exists a need to develop and evaluate alternate desalination technologies, e.g., membrane distillation (MD) which utilizes waste heat. In one variety of MD, direct contact membrane distillation (DCMD), hot brine flows on one side of a gas-filled porous hydrophobic hollow fiber membrane and cold distillate flows on the other side of the membrane. This technique is of interest here. The primary deficiencies of this technique are flux reduction due to long-term pore wetting and reduced brine-side heat and mass transfer coefficients.

To overcome these, this research has made a preliminary investigation of the DCMD process where a number of changes were introduced: (1) The porous hydrophobic hollow fiber membrane has a thin water-vapor permeable hydrophobic microporous coating of a silicone-fluoropolymer plasmapolymerized on the fiber outside diameter on the hot brine side to prevent pore wetting; (2) to increase the brine-side heat transfer coefficient drastically, the hot brine feed is in a rectangular cross flow mode vis-à-vis the hollow fiber membranes; (3) the hydrophobic porous hollow fibers had thick walls and high porosity; (4) the module design ensured that the temperature rise of the cold distillate was minimal. It is known that the vacuum membrane distillation (VMD) technique, wherein there exists vacuum instead of cold distillate flow on one side of the membrane, the other side having hot brine flow, can illuminate many features of the brine side of a DCMD process. Therefore extensive data were obtained for the DCMD as well as the VMD process.

Porous hydrophobic polypropylene hollow fiber membranes had internal diameters between 200 and 330 μm and wall thickness between 50-150 μm. These fibers had different plasmapolymerized microporous coatings of a silicone-fluoropolymer. Module design employed rectangular cross flow. The fiber number in a module was varied between 170-624. The membrane surface area was varied between 113-257 cm^2. The brine feed temperature ranged between 60 and 90 °C in DCMD. At a high feed velocity over the fibers, a water permeation flux as high as 79 kg/m^2-h was achieved in DCMD at 90 °C through the small MXFR #3 module. This indicated that, using appropriate fibers and a reasonable cross flow velocity on the shell side, the water permeation flux can be substantial. No leakage of salt or water was encountered during the extended use of these modules in DCMD or VMD.

The module MXFR #3 built out of larger fibers (330 μm internal diameter (I.D.), 150 μm wall thickness) and a related module MXFR #1 yielded the best DCMD performance. Nitrogen permeation tests through different modules indicated that the fibers in this module had the highest N_2 permeance. An extended-term DCMD test was carried out for a period of 120 hours at 85 °C using the MXFR #3 module. The steady state water vapor flux was found to be 54 kg/m^2-h. The initial time flux decay was likely to be due to a thermal creep in the coatings. Fouling from dirt cannot also be ruled out. DCMD and VMD results suggest that higher gas permeance of the microporous coatings, larger fiber wall porosity and pore size, larger fiber I.D. and appropriate flow rates of the hot brine and the cold distillate are essential to achieving a stable and high value of water-vapor flux in DCMD.

2. Background and Introduction to Potential Solution

Research and development of desalination technologies to increase the availability of cheap and reliable sources of potable water is of significant importance due to the ever increasing population and their needs. Although research and development efforts have focused primarily on existing membrane-based and thermally-driven processes and technologies, there is need for alternative desalination technologies which may potentially be easier to use, cost effective and use energy like low-grade waste heat currently not utilized. Membrane distillation is one such process for desalination.

Membrane distillation (MD) is an evaporation process of a volatile solvent or solute species from a solution (in most cases, an aqueous solution), driven by a difference between its partial pressure over the solution contacting one side of a porous hydrophobic membrane and its partial pressure on the other side of the membrane. When the partial pressure difference through the membrane is created by the direct contacting of a liquid cooler than the feed on the other side of the membrane, the process is called direct contact membrane distillation (DCMD). This is illustrated for a hollow fiber-based process in Figure 1a where the hot brine flows on the shell side of the fiber and the cold distillate flows on the tube side through the fiber bore. When the side of the hollow fiber membrane opposite to the hot brine is subjected to vacuum to develop a partial pressure difference across the membrane, the process is identified as vacuum membrane distillation (VMD). Figure 1b illustrates the VMD process where the hot brine flows on the shell side of the fiber and vacuum is applied on the tube side.

In a MD process, the membrane used must be porous and hydrophobic. Surface tension forces withhold liquids from the pores, and prevent the penetration by the liquids and thus contact between the two liquids in a DCMD process. Generally, the solutions are aqueous and their surface tensions higher than the critical surface tension of the polymer making the membrane. In a DCMD process, the temperature difference, causing a corresponding vapor pressure difference across the membrane, provides the driving force of the membrane distillation process. Evaporation will occur at the solution surface if the vapor pressure on the solution side is greater than the vapor pressure at the condensate surface. Vapors then diffuse through the pores to the cooler surface where they condense. The dependences of mass and heat transport upon different membrane and process parameters involved in membrane distillation have been investigated theoretically (Schofield et al., 1987, 1990a,b; Lawson and Lloyd, 1996a; Martinez-Diez and Vazquez-Gonzalez, 1999).

A system of great research interest in MD is the production of fresh water from saline water. The advantages of membrane distillation for water production by such a method are:

(a) it produces high quality distillate;
(b) water can be distilled at relatively low temperatures (30 to 100 ºC) and low pressure (1 atm);
(c) low grade heat (solar, industrial waste heat, or desalination waste heat) may be used;
(d) the water does not require extensive pretreatment to prevent membrane fouling as in pressure-based membrane processes.

Potential disadvantages of the process are:

(a) the water evaporation rate is strongly controlled by the brine side heat transfer coefficient resulting in a relatively low permeate flux compared to other membrane filtration processes such as reverse osmosis (RO);
(b) over an extended time, there is flux decay and distillate contamination due to pore wetting;
(c) uncertain economic cost.

There are a number of ways to overcome the deficiencies. To prevent pore wetting and long-term flux decay, an extremely thin highly water vapor permeable microporous coating of a hydrophobic silicone-fluoropolymer could be applied on the outside surface of the porous hydrophobic hollow fibers facing the hot brine to make the membrane essentially nonwettable. The resulting configuration for DCMD is illustrated in Figure 1c. The corresponding configuration for VMD is shown in Figure 1d. Secondly, transverse flow of hot brine over this coated fiber surface could be implemented via novel rectangular cross flow module designs to enhance the brine side heat transfer coefficient, reduce temperature polarization and thereby increase the water vapor flux across the membrane.

In Phase I of this project carried out earlier (Sirkar and Qin, 2001), modules having an ultrathin microporous silicone coating on the outside surface of hydrophobic porous polypropylene hollow fibers of smaller diameters were employed. Using a parallel flow Module 4 and high hot water velocity in the fiber bore (Figure 1e) yielded a water flux of 15 kg/m^2-h at 91 °C in VMD. There was no pore wetting during and after a cumulative experimental duration of 1000 hours (among them approximately 400 hours for 1 wt% or 3 wt% brine) without any module washing in between the runs. The ultrathin plasmapolymerized silicone coating on the porous hollow fiber surface was also successful in preventing any pore wetting by hot water or hot saline solutions when these solutions were flowing on the coating side. A large rectangular module having 6000 microporous hollow fibers having an I.D. of 200 μm and outside diameter (O.D.) of 305 μm (polypropylene, Akzo) with an appropriate coating yielded very low water vapor flux in DCMD. Generally, the performance in DCMD for all modules studied was poor in the sense, that the water vapor flux was quite low in the range of 0.01-0.8 kg/m^2-h. It was observed that for the system dimensions the shell side Reynolds number of hot brine achieved under the laboratory conditions was quite low. Further conductive heat loss was substantial. Moreover, the cold distillate temperature was too high at the exit. It meant that much higher cold distillate flow rate was needed to keep its temperature low.

This Phase II research has explored a number of approaches to enhance the actual performance of the DCMD process. The rectangular cross flow module design, the fiber packing and the experimental flow conditions were such as to ensure the achievement of appropriately high Reynolds number in the shell side cross flow of the hot brine. This reduced the temperature polarization on the brine side (Figure 1f). The increased fiber bore diameter, the decreased fiber number and an appropriate distillate flow rate were employed to provide limited temperature rise in the cold distillate under moderate pressure drop. Under these conditions, this research utilized small rectangular hollow fiber modules to study the desalination performance and water vapor flux achieved under DCMD conditions. Vacuum membrane distillation using pure water as well as saline water was also carried out extensively to understand better the DCMD performances.

VMD experiments were done with hot feed through the tube side as well as the shell side. An extended-term study was carried out with one rectangular cross flow module for a continuous period of 5 days. Nitrogen permeation tests of the coated fibers were carried out to correlate the DCMD performances with the resistances of the microporous plasmapolymerized silicone-fluoropolymer coating and the porous fiber.

3. Conclusions and Recommendations

1. Six small hollow fiber modules having rectangular cross flow of hot brine over the outside fiber diameter and cold distillate flow in the fiber bore were successfully studied for DCMD-based water recovery from hot feed brine over a temperature range of 60-90 °C. The fibers had a microporous plasmapolymerized coating of a silicone-fluoropolymer on the O.D.. Under no circumstances, we encountered any salt leakage into the fiber bore distillate streams. Module MXFR #3 was used extensively for more than 400 hrs. This includes a continuous 5-day long DCMD run. Extensive VMD runs with different modules also demonstrated that there was no pore wetting.

Such a conclusion should be tested in future via an extended DCMD run lasting up to 1 month on a continuous basis.

2. A water vapor permeation flux of 79 kg/m^2-hr based on the fiber internal diameter (I.D.) was achieved at 90 °C in DCMD in the module MXFR #3 with the hot brine in rectangular cross flow on the fiber O.D. and cold distillate in the fiber bore.

Such a high flux value was achieved due to the high heat transfer coefficient in the rectangular cross flow of brine, more open microporous silicone-fluoropolymer coating on the fiber O.D., thicker fiber wall reducing conductive heat loss, and a lower cold distillate temperature rise due to higher distillate flow rate in the larger diameter fiber bores which ensured a low distillate pressure drop.

Since the effective cross sectional area for shell-side hot brine flow in the module studied was ~9 cm^2, scaled up modules having a brine flow cross sectional area of 100-200 cm^2 should be studied. The membrane surface area should be increased correspondingly from 120 cm^2 to around 0.2-0.3 m^2.

3. In the 5-day long continuous DCMD run carried out with 85.5 °C brine in module MXFR #3, the water vapor flux decreased from an initial value of ~ 70 kg/m^2-hr to a stable value of ~ 54 kg/m^2-hr. Experiments carried out later under the same conditions yielded a flux of 60 kg/m^2-hr without any module cleaning. Investigative studies are needed to identify the role of dirt, fouling, creep in the coating etc. in causing the observed initial flux drop in DCMD.

4. The performance of module MXFR #1 was somewhat close to that of MXFR #3. Other modules employing smaller fibers having less open microporous silicone-fluoropolymer coatings yielded much poorer performance in DCMD. It is necessary to reproduce the high performance level of MXFR #3 with larger and more number of modules. The fibers to be used have to be studied/characterized in greater detail vis-à-vis their microporous characteristics as well as their fouling tendencies and thermal creep, if any.

The recommendations identified in 1. to 4. above should be implemented in a future project. Further, modules containing 1 m^2 membrane area should be studied; 5-6 such modules in a stack could yield 1 gallon per minute of distillate. That would provide a convenient basis for a future pilot plant study.

4. Work Performed

4.1 Experimental details

4.1.1 Membrane modules

Eight rectangular cross flow hollow fiber modules were obtained from Applied Membrane Technology Inc., Minnetonka, MN, henceforth AMT, Inc. The porous hollow fiber membranes in these modules were plasma-coated with different proprietary recipes by AMT, Inc. so as to compare and optimize the coating process and formulae. The characteristics of the hollow fibers and the membrane modules are listed in Tables 1a and 1b. Among the modules employing larger diameter fibers, MXFR #1 and MXFR #2 represent one pair; MXFR #3 and MXFR #4 represent another pair different from MXFR #1. MXFR #2 and MXFR #4 had some blocked broken fibers. Therefore, modules MXFR #2 and MXFR #4 were not used in any VMD and DCMD measurement. We did not receive modules MXFR #5 and MXFR #8 from AMT; so they are not listed in Table 1b. Figure 2a shows the photograph of such a rectangular cross flow module. A photograph of the fiber arrangement in the modules is shown in Figure 2b.

Since the modules received from AMT, Inc. were only rectangular channels having coated hollow fibers running across and two open faces, we designed and fabricated a diverging section and a converging section to allow the liquid to flow uniformly in cross flow outside of and perpendicular to the fibers. The diverging section and the converging section were two boxes having a curved shape (see Figure 3). Two face plates were made from two flat plastic sheets. On each sheet, 91 smaller holes having a wide size distribution were opened (The hole sizes were such that the holes at the center were smaller, while those further away were progressively larger) (see Figure 4). The design mentioned above ensured that the feed solution flowed uniformly through the shell side of the fibers. The material used for the face boxes and face plates was clear cast acrylic plastic having a reasonable thickness and heat transfer resistance.

Two face boxes and face plates were assembled with a rectangular membrane module channel to constitute the complete device (Figure 5). Neoprene gaskets (1/6″) were used between the face box, the face plate and the module channel on each side to seal the parts together. Hot brine was allowed to enter one face box, then leave the box through the face plate holes which distributed the liquid flow evenly, and then enter the flow channel. On the other side the liquid left the channel through the face plate holes and collected in the face box and then flowed beyond the box and thus the module. By our special design, there was no free space between the faces of the two boxes and the fiber layer. Therefore, the liquid crossed the fiber layer uniformly and perpendicularly to ensure good heat and mass transfer.

4.1.2 Experimental apparatus and procedures

The experimental apparatus was developed such that either the DCMD process or the VMD process could be studied easily. The change from DCMD to VMD or from VMD to DCMD could be easily implemented by operating two three-way valves. A schematic of the apparatus is shown in Figure 6. Figure 7 shows a photograph of the membrane module assembled in DCMD

and VMD system. Figure 8 provides a photograph of the experimental setup of Figure 6. This setup was prepared under Tasks 2, 3 and 4. A summary of the project tasks is provided below to provide a perspective:

Task 1. Develop laboratory-scale cross flow hollow fiber membrane modules having an appropriate coating on the fibers.
Task 2. Study the VMD behaviors of different membrane modules obtained in Task 1.
Task 3. Study the DCMD behaviors of different modules found promising in Task 2.
Task 4. Study the DCMD behavior of a promising module selected from Task 3 for an extended period between 10-30 days.
Task 5. Develop a preliminary cost estimate for DCMD-based desalination of brine.
Task 6. Prepare and submit data, progress reports and a final report.

DCMD: In the experimental setup for DCMD operation shown in Figure 6, deionized water or saline water feed was introduced to the shell side from a reservoir by a digital Masterflex peristaltic pump (Model No. 77601-10 with L/P 82 tubing) at a constant flow rate (the flow rates of the liquid system can be varied between 400-13000 ml/min). The connecting tubing was immersed in the water bath before the feed entered the module. Two HAAKE temperature controllers (Model No. D-76227) maintained the bath temperature at a given value and thus maintained a constant entrance temperature for the hot feed. Outside the membrane module, the feed was circulated to the feed reservoir and was re-warmed.

Deionized water was introduced as a cooling liquid on the fiber lumen side of the module from a reservoir by another digital Masterflex peristaltic pump (Model No. 7518-60) at a constant flow rate. The connecting line was immersed in a Cole-Parmer Polystat refrigerated bath (Model No. 12111-20) at a given low temperature before the water entered the module.

The inlet and outlet temperatures of the hot feed and the cold water were measured by four thermocouples connected to a Cole-Parmer temperature monitor (Model No. 90610-10). The electrical conductivity or the salt concentration of the samples was measured by a conductivity meter (Model No. 115, Orion Research, Beverly, MA).

When the readings of the flow rates of the hot solution, cold distillate water and the four inlet and outlet temperatures reached constant values, it was assumed that the experimental conditions had reached a steady state; then the volume increase in the cooling water reservoir was used to calculate the water vapor flux through the membrane under the given experimental conditions. Water vapor flux was calculated from the following relation:

$$\text{Water vapor flux } \left(\frac{\text{kg}}{\text{m}^2\text{ - h}}\right) = \frac{\text{vol. of water transferred (l)} \times \text{density of water (kg/l)}}{\text{membrane area (m}^2\text{)} \times \text{time (h)}} \qquad (1)$$

Here, the membrane area was calculated based on the hollow fiber inside area: $s = n\pi d_i L$.

VMD: In the experimental setup for VMD shown in Figure 6, hot deionized water or saline water was introduced as a feed to the fiber lumen side or shell side from a reservoir by a digital Masterflex peristaltic pump at a constant flow rate. The feed pipeline was immersed in the water bath before the feed entered the module. The bath temperature was maintained by two temperature controllers at a given level so as to maintain a constant entrance temperature for the hot feed. The exit on the other side of the module was connected to an evacuation system to maintain vacuum by a Fisher Scientific vacuum pump (Model No. M8C). The vacuum was monitored by a J-KEM Scientific digital vacuum regulator (model 200) and controlled by means of a needle valve attached to the bypass loop of the regulator at a preset pressure within ± 1 mm Hg. Two glass vacuum traps (United Lab Glass, Richmond, CA) immersed in two liquid N_2 wells (Dewar flask; Lab Glass Inc., Vineland, NJ) and connected in series to the vacuum pump were used to collect the permeate vapor.

Before the measurement of the water vapor flux, the three-way ball valves attached between the vacuum pump and the vacuum traps were switched to connect the vacuum pump with the inline permeate collector. When the vacuum reached the designated value, the three-way ball valve was switched to the stand-by trap. Then another three-way ball valve, attached between the hollow fiber module and the vacuum trap, was switched over to the stand-by vacuum trap. After stabilization of the vacuum in the stand-by trap (its vacuum was the same as the value in the inline permeate collector), both valves were switched to inline permeate collector at the same time to start to collect the permeate vapor. Permeate vapors were collected for a fixed interval of time in the inline permeate collector. This trap was then isolated from the system for sampling purposes by a set of two three-way ball valves while the stand-by vacuum trap was brought online. The isolated vacuum trap was then removed from the liquid N_2 well and its temperature was allowed to rise up to room temperature. The electrical conductivity or the salt concentration in the samples was measured by a conductivity meter.

The weights of the inline permeate collector were taken before and after permeate collection for calculation of water flux. Water vapor flux was calculated from the following:

$$\text{Water vapor flux } \left(\frac{\text{kg}}{\text{m}^2\text{ - hr}}\right) = \frac{\text{wt. of condensed water (kg)}}{\text{membrane area (m}^2\text{)} \times \text{time(hr)}} \qquad (2)$$

Here, the membrane area based on the fiber inside area was used for the calculation; membrane area $s = n\pi d_i L$.

Leak testing: All membrane modules, listed in Tables 1a and 1b, were tested for leakage before DCMD and VMD measurements. Before the leak tests, each membrane module was activated by circulating deionized water in the shell side and tube side at a very low flow rate and at room temperature for at least 10 hr. Then the module was assembled in the DCMD system. 1 % NaCl solution at 85 °C flowed through shell side at a constant flow rate between 600-2000 ml/min, and deionized water flowed through the tube side at room temperature. The conductivity of the distillate was monitored with increasing saline flow rate. If the conductivity of the distillate water rose evidently with operating time, the test membrane module was leaking.

Otherwise, the test membrane module was leak free. After the DCMD leak testing, the leak-free membrane module from DCMD tests was tested under VMD. The procedure of VMD leak testing was the same as DCMD's except as follows: change the circulating deionized water in tube side under DCMD with vacuum. Presence of water in the vacuum line indicated leakage.

The leak testing indicated that module MXFR #2 was leaking even at a low brine flow rate or inlet pressure; Module MXFR #1 started leaking while the flow rate at the shell side was over 1200 ml/min. The other modules appeared to be good under conditions used in VMD and DCMD. The gauge pressures of the flowing liquids in DCMD tests were around 3 psi (15.6 cmHg gauge).

Gas permeation: A system was also established for the measurement of gas permeance of the coated porous hollow fiber membranes using a gas permeation apparatus (Figure 9). The N_2 gas from the cylinder permeated through the membrane from the tube side to the shell side. The pressures of upstream and downstream were measured by Ashcroft Test Gauge (PT. No. 63-5631). The downstream flow rate of the gas was measured using a soap bubble flow meter. During the permeation measurements, the upstream pressure was maintained at a constant pressure, between 0.1-0.6 psig (0.5-3.1 cmHg gauge). The permeation measurements were made at room temperature. The permeant gas was N_2.

The N_2 permeance of the hollow fiber membranes is related to the measured steady-state permeation rate of nitrogen through the membrane by Eq. (3):

$$\frac{Q_{N_2}}{\delta_M}(permeance) = \frac{P_1 V_1 T_0}{P_0 T_1 \cdot s \cdot \Delta P_{N_2}} \tag{3}$$

In Eq. (3), T_0 = 273.15 K, P_0 = 760 Torr, ΔP_{N_2} corrected to STP is pressure difference across the membrane, s is the inside membrane area, P_1 is the atmospheric pressure, T_1 is the room temperature, V_1 is the volume flow rate of gas through the membrane during measurement at room temperature, Q_{N_2} is the permeability coefficient of N_2 permeation through the membrane of effective thickness δ_M .

Calculation of Reynolds numbers: Reynolds number is normally defined in the following way:

$$\mathrm{Re} = \frac{D \times V \times \rho}{\mu} \tag{4}$$

Where:

Re : Reynolds number; D : characteristic dimension; V : velocity; ρ : density; μ : dynamic viscosity (absolute viscosity).

In Tasks 2, 3 and 4 of this project, the Reynolds numbers of the feed or the distillate flowing through the shell or the tube side were defined as diameter–based Reynolds number (Re_d). In the calculation of Re_d based on Eq. (4), fiber I.D. (d_i) and linear velocity are used for tube side parallel flow, and fiber O.D. and interstitial velocity for shell side cross flow.

Interstitial velocity = brine flow rate/open area for flow through the shell side (5)

The open area for flow through the shell side has been defined at the bottom of Tables 1a and 1b.

Linear velocity = flow rate/open area for flow through the tube side (6)

In the MD literature, boundary layer heat transfer coefficients are almost always estimated from empirical correlations. For laminar flow in a circular tube (i.e. fiber lumen), Sieder-Tate equation is popularly employed (Gryta et al., 1997; Hobler, 1986):

$$Nu = 1.86(d_i \,\mathrm{Re}_d \,\mathrm{Pr}/L)^{0.33}(\mu/\mu_w)^{0.14} \tag{7}$$

where Nusselt number, $Nu = h_p d_i / k$, $\mathrm{Re}_d = (linear\ \ velocity) d_i \rho / \mu$ and the Prandtl number, $\mathrm{Pr} = c_p \mu / k$. Further h_p is the tube side boundary layer heat transfer coefficient, d_i is the tube/fiber I.D., k is the liquid thermal conductivity, μ_W is the liquid viscosity evaluated at the tube-wall temperature, c_p is the liquid heat capacity, and L is the tube length. The viscosity correction factor $(\mu/\mu_w)^{0.14}$ normally is negligible for MD applications (Lawson and Lloyd, 1996b). Equation (7) is suitable for laminar tubular flow conditions (Re_d <2100).

For the calculation of the boundary layer heat transfer coefficient of liquid flowing on the shell side of rectangular cross flow hollow fiber modules, we have not been able to locate any publication relative to this subject. Zukauskas equation is often used in the calculation of the Nusselt number for cross flow over tube bundles in heat exchangers when $10 < \mathrm{Re}_d < 5\times10^2$ (Incropear and Dewitt, 2002; Kreith and Bohn, 2001):

$$Nu = 1.04\,\mathrm{Re}_d^{0.4}\,\mathrm{Pr}^{0.36}(\mathrm{Pr}/\mathrm{Pr}_w)^{0.25}F_c \tag{8}$$

where Nusselt number, $Nu = h_f d_o / k$. Further h_f is the shell side boundary layer heat transfer coefficient, d_o represents the tube/fiber O.D., Pr_w is the Prandtl number evaluated at the tube-wall temperature, F_c is the tube-row correction factor. All properties except Pr_w are evaluated at arithmetic mean of the fluid inlet and outlet temperatures. We report these equations here to provide a basis for using Re_d in reporting our data even though there is a problem due to fibers potentially moving and any irregularity of flow from the entrance section. Further the velocity used in Re_d is the interstitial velocity which takes into account the fiber packing density.

Definitions of heat transfer coefficients: At steady state, the effective heat flux at the two liquid-membrane interfaces (Figure 1f) may be described by

$$Q = h_f A_{rf} (T_f - T_{fm}) = h_f A_{rf} \Delta T_F = h_p A_{rp} (T_{pm} - T_p) = h_p A_{rp} \Delta T_P , \quad (9)$$

where Q is the effective heat flux through the membrane, ΔT_F is the temperature difference between brine bulk temperature, T_f and the temperature of the brine-membrane interface on the feed side, T_{fm}, ΔT_P is the temperature difference between the temperature of the membrane-distillate interface, T_{pm}, and the distillate bulk temperature on distillate side, T_p. In the hollow fiber module, the membrane thickness is comparable with the inside diameter of the fiber. This results in considerable difference between the outside and inside area of the hollow fiber membrane. In this case, a change of the membrane surface area for heat transfer should be taken into account. Here, A_r is the area ratio for the heat transferred through the membrane. Since we have selected the internal diameter-based surface area as our basis, therefore A_{rf} for the interfacial area between the hot brine and the O.D. is (d_o / d_i); the corresponding A_{rp} is (d_i / d_i)=1 .

At the pore mouth on the membrane surface, water from the brine is vaporized; the heat flux transferred by this vapor flux across the membrane is

$$Q_V = h_v A_{r\ln} (T_{fm} - T_{pm}) = h_v A_{r\ln} \Delta T_m = N_V A_{r\ln} \Delta H_V \quad (10)$$

where h_v is the heat transfer coefficient related to the water vapor flux, ΔT_m is the trans-membrane temperature difference $(T_{fm} - T_{pm})$, N_V is the mass flux of water vapor across the membrane and ΔH_V is the heat of vaporization/mass of water. The surface area ratio ($A_{r\ln}$) is defined as ($d_{r\ln} / d_i$) where $d_{r\ln}$ is the logarithmic mean diameter, (($d_o - d_i$) / ln(d_o / d_i))).

Heat is additionally conducted through the nonporous solid polymeric part of the membrane and the gas phase that fills the pores at a rate

$$Q_m = h_m A_{r\ln} (T_{fm} - T_{pm}) = h_m A_{r\ln} \Delta T_m \quad (11)$$

where h_m is the membrane heat transfer coefficient. Further

$$h_m = \varepsilon h_{mg} + (1 - \varepsilon) h_{ms} \quad (12)$$

where ε is the membrane porosity, and h_{mg} and h_{ms} represent the heat transfer coefficients of the vapor/gas within the membrane pores and the solid polymeric membrane material respectively.

The coefficient h_{mg} is generally an order of magnitude smaller than h_{ms}; therefore, the value of h_m is minimized by maximizing the membrane porosity; DCMD process prefers high porosity and high wall thickness membranes so that conductive heat loss through the membrane can be reduced considerably. The plasmapolymerized microporous coating introduces a complication which may be considered an unknown at this time for modeling purposes.

The total effective heat flux across the membrane, Q, is related to Q_V and Q_m by

$$Q = Q_V + Q_m = (h_v + h_m) A_{r\ln} \Delta T_m \tag{13}$$

Since the heat transfer mechanism in DCMD is described as a series of resistances, the overall heat transfer coefficient of the DCMD process, U, is conventionally obtained as a series of resistances defined here with respect to A_{rp}: brine film resistance ($1/h_f$), effective membrane resistance ($1/h_c$) and distillate film resistance ($1/h_p$):

$$UA_{rp} = \left[\frac{1}{A_{rf} h_f} + \frac{1}{A_{r\ln} h_c} + \frac{1}{A_{rp} h_p} \right]^{-1} \tag{14}$$

where

$$h_c = h_m + h_v = h_m + \frac{N_V \Delta H_V}{\Delta T_m} \tag{15}$$

Incorporation of expression (15) in relation (14) leads to the following complex relationship between the overall heat flux Q and the mass flux of water vapor N_V:

$$Q = \left[\frac{1}{A_{rf} h_f} + \frac{1}{A_{r\ln} h_m + N_V A_{r\ln} \Delta H_V / \Delta T_m} + \frac{1}{A_{rp} h_p} \right]^{-1} \Delta T = UA_{rp} \Delta T \tag{16}$$

where ΔT is the bulk temperature difference, $T_f - T_p$; the value of A_r for U depends on the basis of calculation, it can be A_{rf} or A_{rp}, or $A_{r\ln}$. Here we have taken A_{rp} as the basis.

Of the two components of the membrane heat transfer coefficient, h_c, the component h_v is responsible for the most important quantity in DCMD, namely, the water vapor flux. To maximize the latter for a given h_v, ΔT_m should be maximized which in turn will maximize N_V by increasing the temperature T_{fm} which determines the vapor pressure of water at the brine-membrane pore mouth. The value of T_{fm} is usually described via the temperature polarization coefficient (TPC):

$$TPC = \frac{T_{fm} - T_{pm}}{T_f - T_p} = \frac{\Delta T_m}{\Delta T} \tag{17}$$

TPC is the fraction of external applied thermal driving force that contributes to the mass transfer.

If we define an overall boundary layer heat transfer coefficient h via

$$\frac{1}{hA_{r\ln}} = \frac{1}{A_{rf} h_f} + \frac{1}{A_{rp} h_p} \tag{18}$$

then TPC can be defined by

$$TPC = \frac{\Delta T_m}{\Delta T} = 1 - \frac{UA_{rp}}{hA_{r\ln}} \tag{19}$$

Temperature polarization has a negative influence on the productivity of the membrane distillation process as a consequence of the decrease in the temperature of the brine (therefore, the water vapor pressure) on the evaporation surface and its increase on the condensation surface. Ideally, TPC should equal 1, but usually it is lower.

4.2 Experimental Results and Discussion

4.2.1 VMD performances (Task 2)

VMD performances of all leak-free membrane modules listed in Tables 1a and 1b have been determined. The effects of the inlet temperature, feed velocity, module flow configuration (parallel flow or horizontal cross flow), and the brine feeding mode (shell side or lumen side) on the water vapor flux and the outlet temperature were investigated.

The modules MXFR #6 and MXFR #7 have the same support hollow fiber membrane (PP 50/200), but different coatings. The gas permeation experimental results showed that MXFR #7 has smaller final pore dimensions than MXFR #6 (Table 2). So MXFR #6 displayed higher VMD-based water vapor flux than MXFR #7. This shows that the coating in MXFR #7 provides more resistance to water vapor transfer. Typical VMD experimental data are shown in Figures 10 and 11. As the temperature of the hot saline feed was increased, the water permeation flux was increased. Also the water permeation flux increased with an increase in the interstitial velocity of the feed through the shell side.

Normally the liquid flow regime is characterized by its Reynolds number. The effect of Reynolds number of the rectangular cross flow at the shell side on the water vapor flux is summarized in Tables 3 and 4.

Both temperature and the flow rate of the feed solution have obvious effects on Reynolds number. At a given feed temperature, the Reynolds number increases with the increasing velocity of the feed, which causes the water vapor flux to increase (Table 4). Compared to the flow rate, feed temperature has a small effect on the Reynolds number at a given flow rate. That is because there are only limited changes in the density and viscosity of water in the given temperature range. But the effect of temperature on the water vapor permeation flux is striking. The increase of temperature not only increases the Reynolds number, but also drastically increases the water vapor pressure which is the driving force (Table 3). So optimization of the flow rate and feed temperature is an effective way to get high water vapor permeation flux in VMD.

There is another factor, which leads to a high water vapor flux at a high feed flow rate; the increase of feed flow rate decreases the residence time of feed in the module, and increases the feed outlet temperature which increases the driving force and the Reynolds number in a limited way. Figures 12 and 13 illustrate the variation of the feed outlet temperature with its interstitial velocity. It is obvious that the temperature difference between the inlet temperature and the outlet temperature becomes larger with an increase of the inlet temperature. That is because the high water vapor flux at a higher temperature causes more heat removal from the feed solution needed for water evaporation. Based on the same reason, the higher water vapor flux of MXFR #6 is the reason why MXFR #6 has a much higher temperature difference between feed inlet temperature and outlet temperature than MXFR #7 at a given feed inlet temperature.

The effect of the flow mode on VMD performance of membrane modules MXFR #6 and MXFR #7 is summarized in Table 5. Compared to parallel flow, cross flow can reduce temperature polarization considerably and achieve much higher heat transfer coefficients at a similar Reynolds number. So cross flow of hot brine on the outside diameter of the hollow fiber membranes is essential to achieving a high water vapor flux in VMD. The membrane modules show much higher water vapor flux in cross flow than that in parallel flow. (That deionized water was used for parallel flow and 1% brine for cross flow should be of no consequence will be demonstrated soon).

We have summarized the details on all hollow fiber membrane modules, received from AMT Inc. for this project, and their gas permeation properties, and performances in VMD (and DCMD) under particular conditions in Table 2. In all cases the hot deionized water was flowing through the tube side at 85 °C and vacuum was between 60-66 cmHg at the shell side; the water vapor fluxes of these modules displayed a trend identical to their N_2 permeance trend. The gas permeance data illustrate the resistance to N_2 permeation through the microporous coating and the porous substrate. Among those listed in Table 2, the coating opening of MXFR #3 is largest, the fiber porous structure is very open, and its VMD water vapor flux is highest (15.6 kg/m^2-h). These results suggest that high porosity of the hydrophobic support membrane and appropriate hydrophobic coating opening and thickness are quite important for membrane distillation.

Figure 14 illustrates the data obtained using various membrane modules for VMD for hot feed flowing through the shell side at 85 °C. The interstitial velocity of feed was varied from 50 cm/min to 435 cm/min.. D.I. water as well as 1% brine were used. The vacuum level maintained was varied between 60 cmHg and 66 cmHg. Module MXFR #3 yielded a water vapor flux of 46

kg/m^2-h to 71 kg/m^2-h as the Reynolds number was varied from 28 to 95. These water vapor flux values are quite high for a hollow fiber membrane module in VMD. The performances of MXFR #6, MXFR #7, MXFR #9 and MXFR #10 were however much inferior to that of MXFR #3. The difference in water vapor flux is likely to be due to a difference in the resistance consisting of the coating layer and the substrate since MXFR #3 has a much higher N_2 permeation rate than the other four modules (Table 2).

In Phase I Project (Sirkar and Qin, 2001), it was concluded that the water vapor flux is not apparently influenced much by the addition of the salt to the feed (page 8, Final report), as has been concluded in the literature (Lawson and Lloyd, 1996a). An experimental illustration is shown in Figure 14, which also does not provide conclusive evidence that increasing the NaCl concentration of the feed reduces system performance. The experimental error associated with the data is greater than the any observed decrease in performance. The effect of salt concentration over this performance is negligible.

Figure 15 illustrates the variation of water vapor flux in modules MXFR #3, MXFR #6, MXFR #7, MXFR #9 and MXFR #10 with the flow rate of hot deionized water when the feed was flowing on the fiber lumen side at an inlet temperature of 85 °C. It was found that the rectangular cross flow modules MXFR #6, MXFR #7, MXFR #9, MXFR #10 and the parallel flow module Module 4 (Table 2) had water vapor fluxes much lower than those of MXFR #3 whether the feed flowed on the tube side or the shell side in VMD. The module configurations (parallel flow in tube side and cross flow in shell side) did not show significant influence on the fluxes of modules MXFR #6, MXFR #7, MXFR #9 and MXFR #10, which further supports the conclusion that the resistance comes mainly from the membrane for water vapor permeation in these four modules. For MXFR #10, the water vapor flux is almost independent on the feed flow rate especially when the feed flows on shell side. Being quite different from these modules, MXFR #3 not only has a very high water vapor flux for feed flowing on the shell side, but also a high flux value (reaching 17.5 kg/m^2-h) under feed flowing on the tube side at an inlet temperature of 85 ℃. As shown in Tables 1 and 2, the difference between MXFR #3 and the other modules is that it has a larger I.D. and O.D., higher porosity and more open surface (higher N_2 permeance) which allows the hydrodynamics to have a strong influence over the VMD performance of MXFR #3.

Using the thermodynamic properties of water, we can calculate the membrane heat transfer efficiency η as

$$\eta = N_V \Delta H_V s A_{r\ln} / V_{feed} c_p \Delta T_f \qquad (20)$$

Here, V_{feed} is the volume flow rate of the feed, N_V is the water mass flux through the membrane, ΔH_V is the heat of vaporization of water having a specific heat c_p, and ΔT_f is the temperature drop of feed along the module length. We found that in a VMD process, whether the feed passed on the lumen side or the shell side, the heat transfer efficiency was as high as ≥90% (Table 2).

In terms of water quality, whatever the membrane fiber and module configuration, no trace of salt was found in the distillate. VMD is an interesting process to get distillate water from brine and industrial wastewater; however, a separate vacuum pump and a condenser are needed in VMD.

4.2.2 DCMD performances (Task 3)

As described in Task 2, the VMD performances of six modules, namely, MXFR #1, MXFR #3, MXFR #6, MXFR #7, MXFR #9 and MXFR #10 listed in Tables 1a and 1b, were discussed in the previous section. In this section, the DCMD performances of these six rectangular cross flow membrane modules and one parallel flow membrane module (Module 4) used in Phase I Project (Sirkar and Qin, 2001) will be investigated.

(1) Comparison of rectangular membrane module with parallel flow membrane module

Of the membrane modules studied in VMD, we would like to find those which have satisfactory DCMD performances and explore the factors affecting DCMD behaviors of the membrane modules; to that end, we compared the DCMD performances of six rectangular cross flow membrane modules and a parallel flow module (Module 4) under similar experimental conditions in Figure 16 and Table 2.

In the DCMD studies, membrane modules MXFR #3 and MXFR #1 displayed much higher water vapor flux than modules MXFR #6, MXFR #7, MXFR #9, MXFR #10 and Module 4. Under the given experimental conditions, the water vapor flux of module MXFR #3 reached 45 kg/m^2-hr, and the water vapor fluxes of the modules MXFR #6, MXFR #7, MXFR #9 and MXFR #10 are lower than 5 kg/m^2-h. That is an unexpected and highly encouraging experimental result. Larger fiber pores, more open coating, much thicker wall and cross flow design of MXFR #3 and MXFR #1 are likely to be the main reasons for their excellent DCMD performances.

The PP 150/330 fibers in modules MXFR #1 and MXFR #3 have large I.D. (330 μm) which allows these membranes to have high distillate flow rate in the tube side so as to effectively reduce the temperature increase of the cold distillate stream. Meanwhile, the large fiber bore allows the distillate flow pressure drop to remain low. The larger O.D. of MXFR #1 and MXFR #3 (~630 μm, O.D.), compared to the others (~305 μm, O.D.), increases the Reynolds number for the larger fibers at a given velocity (see Table 2). However, the effect on the heat transfer coefficient is in the range of a multiplication factor between 1.3 - 1.9 times.

Ideally the only heat to be transferred across the membrane pores is that needed to evaporate the water vapor across the membrane. In reality, there will be an additional amount of heat transferred by conduction through the membrane. This conductive flux consists of the sum of the conductive heat flux through the nonporous part of the polymeric membrane and the conductive heat flux through the gas in the pores of the membrane. The loss due to this conductive flux directly results in a decrease of temperature of the hot feed solution and increase of temperature

of the cold distillate water flowing in the module. It is known that membrane distillation is a process driven by temperature difference. The DCMD performance of membrane module should be improved by increase of the membrane wall thickness due to the decrease of conductive heat flux. The experimental results are shown in Table 2. Clearly large fibers in modules MXFR #1 and MXFR #3 have smaller conductive heat loss and much higher water vapor fluxes.

Gas permeation measurements indicated that the N_2 permeance of MXFR #3 reached 0.196 $cm^3(STP)/cm^2 \cdot s \cdot cmHg$ which is much higher than those of MXFR #6, MXFR #7, MXFR #9, MXFR #10 and Module 4 (0.005-0.013 $cm^3(STP)/cm^2 \cdot s \cdot cmHg$) . The value of gas permeance directly reflects how open are the pores of hollow fiber as well as those in the polymeric coating. The open area for water vapor molecule permeation not only includes the open area of the pore but also the water vapor permeability of the coating membrane covering the open pore mouth of the hollow fiber. A suitable opening and a very thin coating are important for getting very high water vapor flux in DCMD performance. That MXFR #3 has a much higher water vapor flux than others appears to be explainable from this point of view.

Based on the above analysis, it is concluded that, comparing the water vapor flux of the modules having different flow patterns, the DCMD performance was improved drastically by the rectangular cross flow. The cross flow of hot feed solution over the fibers on the shell side increases the heat transfer coefficients drastically at similar Reynolds numbers with parallel flow. Also it is known from the literature of membrane contactors employing microporous hydrophobic hollow fibers (Wickramasinghe et al. (1992); Yang and Cussler (1986)) that cross flow can increase the mass transfer coefficient by a factor of 5 - 7 at the same Reynolds number.

All cross flow membrane modules showed much higher water vapor fluxes in DCMD than the parallel flow membrane module. Compared to modules MXFR #6, MXFR #7, MXFR #9 and MXFR #10, the hollow fiber membranes in modules MXFR #1 and MXFR #3 have a much thicker wall allowing MXFR #1 and MXFR #3 to have a lower conductive heat flux. Further they have a larger fiber I.D. which allows higher tube side flow rate so that the distillate temperature rise is lower, and higher Reynolds number to increase the heat transfer coefficient and reduce the temperature polarization. More importantly they have a more open (or thin) coating and high porosity of fibers allowing MXFR #1 and MXFR #3 to have a very high effective open area for water vapor transport through the membrane from the shell side to the tube side. All of these factors contributed to modules MXFR #1 and MXFR #3 displaying excellent DCMD performances.

(2) Module MXFR #3

Because of the excellent DCMD performances of MXFR #3, research on membrane module MXFR #3 was emphasized. In this study, the relations between the feed temperature, feed velocity and water vapor permeation flux were investigated. The variation of water vapor permeation flux with the interstitial velocity of hot saline (1%) as feed at different brine inlet temperatures is shown in Figure 17.

For a given brine temperature, an increase of interstitial velocity in cross flow on the shell side leads to an increase of Reynolds number which maximizes the brine–side boundary layer heat transfer coefficient. Higher heat transfer coefficient leads to higher sensible heat loss which supports the increased water vapor permeation flux. The effect of feed flow rate is more obvious especially at high temperatures. Meanwhile, the increase of feed flow rate decreases the residence time of feed in the module, and increases the feed outlet temperature which increases the vapor pressure-based driving force and the Reynolds number. Figure 18 indicates the variation of feed outlet temperature with its interstitial velocity. It is obvious that the temperature difference between inlet temperature and outlet temperature becomes larger with an increase of inlet temperature at a given velocity on the shell side. That is because the high water vapor flux at a high temperature causes more heat removal from the feed solution for water evaporation.

Based on the data of Figure 17, the effect of feed inlet temperature on water vapor flux is illustrated in Figure 19 for the module MXFR #3. Normally the feed temperature has a small effect on the Reynolds number at a given flow rate. That is because there are only limited changes in the density and the viscosity of water in the given temperature range. But the effect of temperature on the water vapor permeation flux is striking in our situation. The increase of temperature drastically increases the water vapor pressure which is the driving force. That is why the water vapor flux rises almost exponentially with temperature as the temperature rises. This plot includes a data point at 90 °C; this data point was not present in Figure 17.

The effect of the flow rate of the cold distillate water flowing through the tube side of module MXFR #3 on the water vapor flux in DCMD is illustrated in Figure 20. The increase of the distillate flow rate makes the distillate temperature rise much less, which maintains thereby the needed ΔT for higher water vapor permeation flux. The water vapor flux rises with an increase in the flow rate of the cold water. But the extent of the increase of water vapor flux is much lower than that due to an increased brine flow rate in the shell side. This is because the conditions of this so-called "temperature polarization" on the cold distillate side are not as critical; the water vapor pressure at the relatively low distillate temperatures changes only slowly with temperature.

The effect of D.I. water and saline solution as feed on the vapor permeation flux was compared. Under the same experimental conditions (membrane module: MXFR #1; feed: D.I. water or 1% NaCl solution; inlet temperature: 80 °C; interstitial velocity: 50 cm/min on the shell side; distillate: D.I. water, inlet temperature: 16 °C, velocity: 980 cm/min on the tube side), the vapor permeation flux in the case of saline (1% NaCl) flowing on shell side is 21.7 kg/m^2-hr, which is slightly lower than that (23.0 kg/m^2-hr) obtained when D.I. water was used as feed. The primary reason is that the salt in water leads to a small decrease in water vapor pressure. A minor effect is also due to the fact that NaCl in water changes the Reynolds number a bit.

In this project the effect of flow rate of the brine flowing through the shell side and the feed temperature on the water vapor flux of membrane modules MXFR #9 and MXFR #10 also were investigated (Figures 21 and 22). These modules had higher N_2 permeances than MXFR #6 and MXFR #7 and therefore were of interest over a wider ranger of feed temperatures. As expected, increased flow rate increases the water vapor flux drastically. However, the magnitudes of the water fluxes are still quite low.

4.2.3 DCMD experiments for an extended period (Task 4)

Based on the results from Task 3, the membrane module MXFR #3 was employed for an extended DCMD run in Task 4 in April, 2002. A feed of 1% hot brine was circulated through the shell side of module MXFR #3 and the feed reservoir. Similarly, cold D.I. water was recirculated as the distillate stream through the lumen, the distillate reservoir and the thermostat shown in Figure 6. Figure 23 represents the variation of water vapor flux with the operating time. For a brine feed at 85.5 °C, this experiment lasted five days. The membrane performance was not completely stable until the experiment was run for 90 hr. The stable water vapor flux was 54 kg/m^2-h. There was a reduction of 23% in the water permeation flux. Although the role of dirt etc. depositing on the membrane surface can not be ruled out, a possible reason for this decrease of water vapor flux is the thermal creep in the membrane and coating material with time around the mouth of the partially covered pore at a high temperature. We have observed that the module MXFR #3 displayed a significantly higher DCMD flux of H_2O vapor (~ 60 kg/m^2-h) at the beginning of a new experiment after the 5-day long extended-term run was over. We did not undertake any cleaning of the module after the extended-term run. The conductivity of the cold distillate was monitored during this extended experiment. The concentration of salt was always less than 8 mg/l, which indicates that the membrane pores were not wetted by the hot brine during this experiment. No bacterial stain was observed in the membrane module or the brine reservoir during the 5-day experiment. Generally, bacterium can not grow in water at 85 °C. However, the pressure drop in the cold distillate water passing through the lumen side of the module was slightly increased (by 25 %). This indicates the possibility of dirt build up in the hollow fiber tube sheet. In the absence of any prefiltration, flow reversal should clean it.

Membrane module MXFR #3 was used since May, 2002 for around 400 hrs. Till the end of August, 2002, it was continually used for VMD and DCMD tests. Under identical experimental conditions used in earlier experiments for VMD and DCMD, MXFR #3 showed essentially similar performances, except that the color of the fibers included in module MXFR #3 became slightly yellowish from white (see Figure 24). We believe that this was caused by some dirt depositing on the coated section due to whatever reasons although thermal effects can not be ruled out. Since the bulk of the area of the open mouth of the pore was covered by a plasmapolymerized coating, and the H_2O vapor flux was predominantly through the remaining open area of the pore, the water vapor flux could not be reduced substantially due to the dirt depositing unless the pores get blocked by these deposits. An effective cleaning method will be developed in future work.

During this study, it was observed that some of the fibers in MXFR #6, MXFR #7, MXFR #9 and MXFR #10 got together during and after the DCMD and VMD runs. Such conditions were not visible in MXFR #1 and MXFR #3 modules. Typical photographs are shown in Figures 24 and 25. In the polar liquid phase of water, the nonpolar fibers tend to be together to reduce the surface free energy by affinity on the surface of the hollow fibers. Two opposing factors-packing fraction and the outer diameter of fiber-affect the extent of stickiness. Small O.D. fibers assembled with a higher packing fraction in the module can easily come together in water. On the contrary, the fibers in MXFR #3, having a larger O.D. (630 μm) and packed with a smaller

packing fraction (0.12), are separated from each other. Of course, the sticking of fibers would decrease the effective surface of the membrane for water permeation, and affect MD performance negatively. How to reduce sticking between fibers will be studied further. The role of a fiber mat with a spacer in between each fiber as currently used in Celgard hollow fiber modules should be explored.

In conclusion, six rectangular cross flow membrane modules were studied in VMD and DCMD. The MD performances were improved drastically by using these modules having cross flow compared to parallel flow. The membrane module MXFR #3 prepared from fibers with larger I.D., larger wall thickness and more open plasmapolymerized silicone-fluoropolymer coating displayed excellent VMD and DCMD performances. Its water vapor flux reached as much as 69 kg/m^2-h at 85 °C and 79 kg/m^2-h at 90 °C in DCMD. These are much higher than any published data for hollow fiber modules. The silicone-fluoropolymer coating provides effective capacity to protect the membrane against fouling. In many runs covering over 400 hours after the 120 hr extended run, we did not observe any salt leakage. The membrane performance demonstrated very good stability.

4.2.4 Cost estimate (Task 5)

A brief comparison of seawater desalination by reverse osmosis (RO) and the proposed direct contact membrane distillation (DCMD) process with respect to the production cost is provided in this section. For our basis of calculation, we assume a purified water production rate of 1,000,000 gal/day (3800 m^3/day). The values for RO are taken from Ray (2001). Other references include Peters and Timmerhaus (1991) and Mulder (1991).

The calculation of production cost is normally based on the capital cost and operating cost. The cost categories for capital and operating costs used in this estimation are shown in Table 6. For the comparison between RO and DCMD, the following assumptions were employed:

(1) Both RO and DCMD desalination plants have the same production rate---1,000,000 gpd.
(2) RO: operating pressure 1000 psi, 30% recovery, feed flow rate 2.3 kgal/min (=0.15m^3/s), energy recovery 30%.
DCMD: operating pressure 5 psi, 30% recovery, feed flow rate 2.3 kgal/min (=0.15m^3/s).
(3) The costs of some capital items --- site development, water, utilities, construction overhead and contingency, and some operating costs --- membrane replacement, labor, spare parts and filters in RO application are the same as those in DCMD.
(4) Both RO membrane and DCMD membrane have the same price ($/m^2). The permeation flux of DCMD is 1.5 times higher than RO. Estimated membrane lifetime is 3 years.
(5) In DCMD, there are two special situations:
(a) An initial amount of cooled distillate water flows on the distillate side. This water gets heated up as it collects the condensate. A fraction of this heated distillate is taken out as product. The rest is cooled in a heat exchanger by cooling water which is cooled down again by means of a cooling tower. Thus additional costs involved include those of (1) distillate heat exchanger; (2) cooling tower and (3) cooling water lost by evaporation in cooling tower.

(b) On the hot brine side, the exiting hot brine temperature is sufficiently lowered. An amount of fresh hot brine is added to it and then this brine is heated up in a heat exchanger by the waste heat source so that it can be fed again to the membrane stack. We have assumed 30% recovery; we can go for even higher recovery. However, it will require a few passes. The costs involved are (1) brine heat exchanger; (2) additional pumping cost.

The values in Table 6 indicate that the total production cost of water by DCMD process is only $2.97/1000 gal which is about half of that for the RO process due to the low pressure operation of DCMD process, high water vapor flux and good anti-fouling properties of the DCMD membrane and process. Compared to the RO process widely used in desalination industry, the salt content of water made from our current DCMD system is <20 ppm, but the salt content in water got from single-stage RO system is > 200 ppm. Therefore, it is prospective to apply the novel technology in industrial desalination.

Note: recent cost reports for water treatment process showed that the production cost of water by RO was $4.77/1000gal (Cost Model, Program for PC, Task E, D-8230 WaTER Desalination and Water Purification Research and Economic Program, Reclamation's Website, http://www.usbr.gov/pmts/water/desal.html, 2002-2003).

5. Analysis of Results and Commercial Viability of the Project

An analysis of the results obtained in the project indicates the following:

1. The increase of shell-side hot brine velocity over the hollow fibers in cross flow substantially increases the water vapor flux. A four-fold increase in the interstitial velocity (Figure 17) produces, for example, more than two-fold flux increase at higher feed inlet temperatures. Higher velocity leads to higher heat transfer coefficient which reduces the temperature polarization; the latter in turn increases the water vapor pressure of the brine drastically and thereby the driving force for water permeation.

2. The extent of openness of the microporous silicone-fluoropolymer coating on the O.D. of the hydrophobic porous polypropylene hollow fiber is very important for the achievement of a higher water vapor flux. The higher the N_2 permeance of such a coating, the higher is the water vapor flux. Yet there was no salt leakage through such a coating. Optimization of the permeance of this coating and a long-term test of its nonwetting characteristics is in order.

3. Thicker and more porous hollow fiber wall leads to a lower loss of the brine enthalpy via heat conduction through the polymeric part of the fiber wall.

4. Very high water vapor fluxes in the range 30-80 kg/m^2-hr are achievable now in DCMD using rectangular cross flow, larger hollow fibers having a more open microporous silicone-fluoropolymer hydrophobic coating and appropriate Reynolds numbers in the brine flow and the cold distillate flow. Such fluxes if sustained on a long-term basis and on a large scale will considerably increase the commercial viability of DCMD for water desalination.

5. The flux decrease during the initial period of a 5-day long extended DCMD run needs to be investigated. What is the role of foulants, dirt etc.? What is the role of a thermal creep if any? A proper assignment of the role of each such potential cause will substantially aid the commercial potential of the DCMD technology of this project.

6. A fiber mat arrangement using an appropriate spacer between the fibers if used to prepare the hollow fiber bundle may prevent clumping of the fibers via hydrophobic surfaces liking each other in an aqueous environment. Commercial hollow fiber modules (e.g. Celgard Inc.) already use such a structure in their cross flow Liquicel® modules.

7. For potential commercial application of this technology, much larger membrane modules having the required effective surface area should be investigated in future.

References

Gryta, M., M. Tomaszewska, A. W. Morawski, *Membrane distillation with laminar flow*, Separation and Purification Technology 11, 93-101, 1997.

Hobler, T., *Heat Transfer and Heat Exchanger*s, PWN, Warsaw, 1986.

Incropear, F. P., D. P. Dewitt, *Chapter 7. External flow, in Introduction of Heat Transfer,* Fourth Edition, John Wiley & Sons, New York, 2002, pp.363-342.

Kreith, F., M. S. Bohn, *Chapter 7. Forced convection over exterior surfaces, in Principles of Heat Transfer,* Six Edition, Brooks/Cole, Pacific Grove, CA., 2001, pp.421-483.

Lawson, K. W., and D. R. Lloyd, *Membrane distillation, II. Direct contact MD,* J. Membr. Sci., 120, 123-133, 1996a.

Lawson, K. W., and D. R. Lloyd, *Membrane distillation, I. Module design and performance evaluation using vacuum membrane distillation,* J. Membr. Sci., 120, 111-121, 1996b.

Martinez-Diez, L., and Mi. I. Vazquez-Gonzalez, *Temperature and concentration polarization in membrane distillation of aqueous salt solutions,* J. Membr. Sci., 156, 265-273, 1999.

Mulder, M., *Basic Principles of Membrane Technology*, 2nd Ed., Kluwer Academic Publishers (1991).

Peters, M.S. and K. D. Timmerhaus, *Plant Design and Economics for Chemical Engineers,* 4th Ed., McGraw Hill, New York, 1991.

Ray, R., *Membrane Handbook* (Eds. W. S. Ho, and K. K. Sirkar), Chapter 25, Kluwer Academic Publishers, Boston (2001).

Schofield, R. W., A. G. Fane, and C. J. D. Fell, *Heat and mass transfer in membrane distillation,* J. Membr. Sci., 33, 299, 1987.

Schofield, R. W., A. G. Fane, and C. J. D. Fell, *Gas and vapor transport through microporous membrane. I. Knudsen-Poiseuille transition,* J. Membr. Sci., 53, 159-171, 1990a.

Schofield, R. W., A. G. Fane, and C. J. D. Fell, *Gas and vapor transport through microporous membrane. II,* J. Membr. Sci., 53, 173-185, 1990b.

Sirkar, K. K and Y. Qin, "*Novel Membrane and Device for Direct Contact Membrane Distillation Based Desalination Process",* Desalination Research and Development Program Report No. 87, 2001.

Wickramasinghe, S. R. J., M. J. Semmens and E. L. Cussler, *Mass transfer in various hollow fiber geometries,* J. Membr. Sci. 69, 235-250, 1992.

Yang, M. C., E. L. Cussler*, Designing hollow-fiber contactors,* AIChE Journal 32 (11), 1910-1916, 1986.

Table 1a. Details of the hollow fibers and the membrane modules used: larger fibers

Particulars	MXFR #1	MXFR #2	MXFR #3	MXFR #4
Support membrane type	PP 150/330 Accurel MEMBRANA			
Support membrane	Polypropylene			
Fiber O.D., μm	630			
Fiber I.D., μm	330			
Wall thickness, μm	150			
Maximum pore size, μm	0.60			
Membrane porosity, %	~60 - 80			
Coating	*Silicone fluoropolymer			
Arrangement of fibers	Staggered			
No. of fibers	(2×20+12×19) = 268	(2×20+12×19)-15(broken)= 253	10×18=180	10×18-10 (broken)=170
Effective fiber length, cm	6.4			
**Effective membrane surface area, cm^2	178	168	119	113
***Effective cross-sectional area for shell side liquid flow, cm^2	7.94		8.74	
Rectangular module frame (internal dimensions)	Length: 6.4 cm, width: 2.5 cm, height: 1.8 cm			
Packing fraction	0.18	0.17	0.12	0.12
Shell side flow mode	Rectangular cross flow			
Fabricated at	AMT Inc. Minnetonka, MN			

* MXFR #1 and MXFR #2 represent one pairing; MXFR #3 and MXFR #4 represent another pairing different from MXFR #1. The coating compositions are proprietary to AMT Inc..

** Based on fiber internal diameter.

*** Based on open area for flow = frame cross sectional area (6.4×2.5 cm^2) – fiber projected area (no. of fibers in one layer × fiber O.D. × length of fiber cm^2).

Table 1b. Details of the hollow fibers and the membrane modules used: smaller fibers

Particulars	MXFR #6	MXFR #7	MXFR #9	MXFR #10
Support membrane type	PP 50/200 Accurel MEMBRANA			
Support membrane	Polypropylene			
Fiber O.D., μm	305		397	
Fiber I.D., μm	200		280	
Wall thickness, μm	52.5		50	
Maximum pore size, μm	Unknown		~ 0.2	
Membrane porosity, %	60		Unknown	
Coating	*Silicone fluoropolymer			
Arrangement of fibers	Staggered			
No. of fibers	13×48= 624	13×48= 624	12×38= 456	12×38= 456
Effective fiber length, cm	6.4	6.4	6.4	6.4
**Effective membrane surface area, cm^2	251	251	256.6	256.6
***Effective cross-sectional area for shell side liquid flow, cm^2	6.63		6.34	
Module frame (internal dimensions)	Length: 6.4 cm, width: 2.5 cm, height: 1.8 cm			
Packing fraction	0.10		0.13	
Shell side flow mode	Rectangular cross flow			
Fabricated at	AMT Inc. Minnetonka, MN			

* The coating of MXFR #6 and MXFR #7 runs differ in the ratio of silicone/ fluoropolymer mixture. Also MXFR #9 and MXFR #10 have different coating formulae. The coating compositions are proprietary to AMT Inc..

** Based on fiber internal diameter.

*** Based on open area for flow = frame cross sectional area (6.4×2.5 cm^2) – fiber projected area (no. of fibers in one layer × fiber O.D. × length of fiber cm^2).

Table 2. Parameters of the hollow fiber membrane modules and gas permeation properties and performances in VMD and DCMD

Particulars	MXFR #1	MXFR #3	MXFR #6	MXFR #7	MXFR #9	MXFR #10	Module 4*
Support membrane type	PP 150/330	PP 150/330	PP 50/200	PP 50/200	PP 50/280	PP 50/280	PP 50/200
Coating	Silicone fluoropolymer						Silicone
Shell side flow mode	Cross flow						Parallel flow
Permeance of N_2, cm^3 (STP)/cm^2·s· cmHg**	0.153	0.196	0.006	0.005	0.011	0.009	0.013
F(VMD-tube), kg/m^2-h (Re_d)***	---	15.6 (136)	9.8 (82)	7.3 (83)	10.4 (118)	9.5 (118)	11.6 (83)
F(VMD-shell), kg/m^2-h (Re_d)****	---	65.0(57)	12.0(30)	8.8 (33)	7.2(39)	6.8(38)	---
η (VMD-average membrane heat transfer efficiency) , %[+]	---	95%	92%	94%	92%	93%	---
DCMD performance(below):[++] Re_d (tube side)	65	68	42	41	50	52	31
Re_d (shell side)	54	58	29	28	35	38	33
Pressure drop (tube side), psi	1.0	1.0	1.5	1.5	1.4	1.3	3.0
Conductive heat flux, kcal/m^2s[+++]	3.5	3.1	5.3	4.9	5.6	5.8	---
F(DCMD), kg/m^2-h [++++]	32.9	41.4	3.9	2.7	1.0	2.9	0.2

* Module 4 was used in Phase I Project (Sirkar and Qin, 2001).

** Experimental conditions: Temperature: 25.5 °C; atmospheric pressure: 76 cmHg; N_2 inlet: tube side; N_2 outlet: shell side.

*** F (VMD-tube): Water vapor flux (VMD), experimental conditions: deionized water (85 °C) as feed flowing through tube side at 900 cm/min of linear velocity; vacuum (60-66 cmHg) at shell side.

**** F (VMD-shell): Water vapor flux (VMD), experimental conditions: saline (1% NaCl at 85 °C) as feed flowing through shell side at around 200 cm/min of interstitial velocity; vacuum (60-66 cmHg) at tube side.

[+] η (VMD-average membrane heat transfer efficiency) = heat used for evaporation of water/total heat loss of feed flowing through membrane module (Equation 20).

[++] DCMD: shell side: 1% saline water at 85 °C (inlet temperature) at 200 cm/min of interstitial velocity; Tube side: DI water at 15 -17 °C (inlet temperature) at 766 cm/min of linear velocity.

[+++] Conductive heat flux = (heat transfer rate from the increase of temperature in the tube side - heat transfer rate for evaporation of water)/effective membrane surface area. It is supposed that the heat loss through module faces in the tube side is negligible.

[++++] F (DCMD): Water vapor flux (DCMD).

Table 3. Effect of temperature on the water vapor flux in VMD of module MXFR #6 at one shell side brine velocity

Inlet temperature (°C)	60	70	80	89
nolds number (shell side)	32.2	36.5	42.7	43.9
H_2O Flux (kg/m^2-hr)	4.45	7.28	11.2	14.7

Feed: 1% NaCl solution flowing on shell side, brine interstitial velocity: 297 cm/min (brine flow rate: around 1967 ml/min). Vacuum: 63-66 cmHg in tube side.

Table 4. Effect of shell side Reynolds number on the water vapor permeation flux of membrane in VMD of module MXFR #6

Interstitial velocity (cm/min)	61	119	235	297
Reynolds number (shell side)	8.3	16.3	32.3	42.7
H_2O flux (kg/m^2-hr)	8.69	9.17	9.97	11.2

Feed: 1% NaCl solution flowing through shell side, inlet temperature: 80 °C; Vacuum: 63-66 cmHg in tube side.

Table 5. Effect of parallel flow and cross flow on water vapor flux in VMD performance

Flow mode		Parallel flow (tube side)*		Cross flow (shell side)**	
Module		MXFR #6	MXFR #7	MXFR #6	MXFR #7
Hot stream flow rate, ml/min		97	97	1960	1960
Linear	Velocity, cm/min	495	495		
Interstitial				295	295
Reynolds number		43.4	43.4	43.4	43.4
Water vapor flux, kg/m^2-h		7.5	6.2	13	9.9

* Feed: deionized water at 85 °C flowing through tube side; Vacuum: 63-66 cmHg at shell side.

** Feed: 1 % NaCl solution at 85 °C through shell side; Vacuum: 60-66 cmHg at tube side.

Table 6. Summary of representative costs for RO treatment and DCMD treatment

Cost category	RO*	DCMD
CAPITAL COSTS ($/gal/day)		
Direct		
Site development	0.10	0.10
Water	0.09	0.09
Utilities	0.16	0.16
Equipment**	3.34	2.18
Land***	---	---
Other	---	---
Total direct capital costs	3.69	2.53
Indirect		
Construction overhead	0.44	0.44
Contingency	0.37	0.37
Other	---	---
Total indirect capital costs	0.81	0.81
Total capital costs	4.50	3.34
OPERATING COSTS ($/1000gal)		
Energy****	1.34	0.37
Membrane replacement	0.41	0.41
Labor and overhead	0.30	0.30
Spare parts	0.09	0.09
Chemicals	0.16	0.08
Filters	0.05	0.05
Cooling water	---	0.10
Other (ion exchange beds)	---	---
Total operating costs	2.35	1.40
Capital recovery costs*****	2.13	1.57
Total production costs ($/1000gal)	4.48	2.97

*Quoted from Ray in Membrane Handbook (2001), p368.

** Categories of equipment costs ($/gal/day)

Component	RO	DCMD
Pretreatment①	0.5	0.3
Membrane module	0.5	0.35
Pumps②	0.8	0.04
Controls, pressure vessels, electrical subsystems, heat exchangers, power recovery system③	1.2	1.15
Shipping and installation	0.17	0.17
Equipment related engineering	0.17	0.17
Total	3.34	2.18

① Pretreatment cost of seawater for DCMD is much lower than that for RO because almost no chemical treatment is needed in DCMD application.

② Reference: Bureau of Reclamation Letter (Denver Federal Center) on June 23, 1999.

③ Here we have found that the cost of all items except energy recovery system (used in RO process) is $0.6/gal/day. The cost calculations for heat exchangers and cooling tower (used in DCMD process) are based on the most recent experiments.

The stable (average) water vapor flux: 40 kg/m^2-h; total membrane area for the production of 1 million gallon/day: 157708(kg/h)/40(kg/m^2-h)=3943m^2; total number of modules (4×0.2864m^2/ module): 3943(m^2)/(0.2864×4)(m^2/module)=3440; feed flow rate on the shell side: 3440×25(l/min) = 86000(LPM) = 1.4(m^3/s); distillate flow rate on the tube side: 3440×(2.6×4)(l/min) = 35800(LPM) = 9460(GPM) = 0.6(m^3/s). (Module area calculation and flow rates based on projection from present system).

(a) Cost of cooling tower: $0.2 million (Peters and Timmerhaus (1991), Figure B-6, page 810).

Cost of cooling water $0.10/kgallon (Peters and Timmerhaus (1991), Table 5, page 815).

(b) Cost of heat exchangers

Feed-shell side: brine water would be heated from 75 °C to 90-95 °C by steam through this heat exchanger if we need to extract more water by multipass arrangement. This is not needed for single pass.

Heat flux: 86000(LPM)×1000(g/l)×15(°C)×1(cal/g °C) = 3×10^8(Btu/h) (Note: 1Btu = 252cal). Assume overall heat transfer coefficient = 500 Btu/h-ft^2-^oF (Peters and Timmerhaus (1991), Table 6, page 601).

Surface area of heat exchanger: 3×10^8(Btu/h)/(500(Btu/h-ft^2-^{o}F)×27(^{o}F)) = 2×10^4 ft^2

(Temperature difference: 27 ^{o}F)

Cost: $\$2\times10^5$ (Peters and Timmerhaus (1991), Figure 15-14, page 616)

Distillate-shell side: distillate would have to be cooled from 85 °C to 30-40 °C by cold water from the cooling tower.

Heat flux rate: 35800(LPM) × 1000(g/l) ×50(°C) ×1(cal/g °C) = 4.2 ×10^8(Btu/h)

Surface area of heat exchanger: 4.2×10^8(Btu/h)/(400(Btu/h-ft^2-^{o}F)×90(^{o}F)) = 1.2×10^4 ft^2
(note: overall heat-transfer coefficient from water to water = 400(Btu/h-ft^2-^{o}F); average temperature difference: 90 ^{o}F)

Cost: $\$1.5\times10^5$ (Peters and Timmerhaus (1991), Figure 15-14, page 616)

Total capital cost for the cooling tower and heat exchangers: $\$(2+2+1.5)\times10^5 = \$5.5\times10^5$
The cost in \$/gallon/day: 5.5×10^5(\$)/10^6(gallon/day)) = \$0.55/gallon/day

*** Normally the land-related costs are negligible.

**** Energy costs include costs for pumps for feed well, high-pressure pumps, cooling, heating, pretreatment system and instrumentation. Suppose industrial waste heat is available; the heat cost can be neglected in DCMD. The dominant energy cost in most installations is for the high-pressure pumps in RO applications; DCMD pumps are cheap low pressure centrifugal pumps.

The representative energy costs can be calculated for a single-stage system using the equation

$$E_P = \frac{q_v \Delta P}{\eta}$$

where q_v = flow rate (m^3/s); ΔP = pressure difference (Pa); η = efficiency of pump and motor (%)

RO: consumption of energy $E_0 = \dfrac{1000(psi)\times 6.9\times10^3(Pa/psi)\times 0.15(m^3/s)}{0.65} = 1592(kW)$

Recovery of energy = 1592(kW) × 30% = 477.6 (kW)
So the total energy consumption = 1592(kW) – 477.6(kW) = 1114.4 (kW)
Energy cost of 1000 gallon water produced =

$$\frac{1114.4(kW)\times 24(hr)\times 0.05(\$)}{1000(gallon)} = 1.34(\$)/kgallon$$

Here pressure difference = 1000 psi; 1 psi=6.9 × 10^{3}Pa; η = 0.65; electricity price = \$0.05/(kW·hr).

DCMD: (1) Feed and distillate flowing through the membrane modules:
Shell side consumption of energy for 5 psi pressure drop

$$E_0 = \frac{5(psi)\times 6.9\times10^3(Pa/psi)\times 1.4(m^3/s)}{0.65} = 74.3(kW)$$

Energy cost of 1000 gallon water produced =

$$\frac{74.3(kW)\times 24(hr)\times 0.05(\$/kW\cdot hr)}{1000(gallon)} = 0.09(\$)/kgallon .$$

Based on a similar calculation, the energy cost of distillate flowing on tube side is found to be \$0.04/kgallon.

Here the pressure drop on each of tube side and shell side = 5 psi.

(2) Heat exchangers and cooling tower

For the heat exchanger for the shell side brine, only one side needs pump due to low pressure waste steam placed on the other side. The maximum energy cost is \$0.09/kgallon.

For tube side heat exchanger, it is supposed that the flow regimes are similar to the DCMD membrane modules. Therefore, the energy cost for both shell and tube sides should be \$0.09 + \$0.04 = \$0.13/kgallon.

For the cooling tower, operating pressure should be much lower than those of heat exchangers. It is reasonable to set the energy cost equal to \$0.02/kgallon.

Total cost for energy: \$0.37/kgallon.

***** Capital recovery costs = $\frac{(total\ \ capital\ \ cost)\times 1000\times i\times\left[1+(i/100)\right]^{r}}{365\times(100-Dt)\times\left[(1+i/100)^{r}-1\right]}$

where r is system lifetime (yr), i is the annual interest rate (%), and Dt represents downtime (%). A system lifetime (exclusive of membrane replacement) of 15 years, an interest rate of 12 %, and a downtime percentage of 15 % are used as representative values.

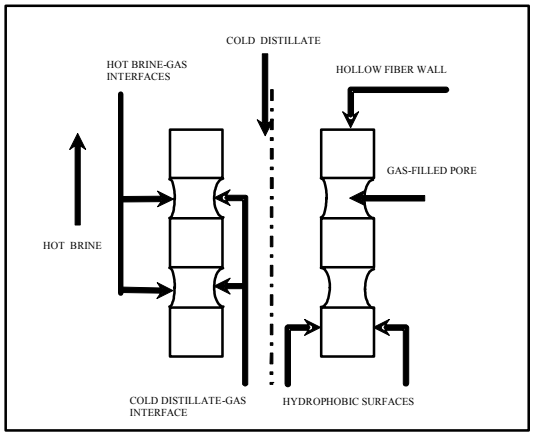

Fig. 1a. Conventional Direct Contact Membrane Distillation

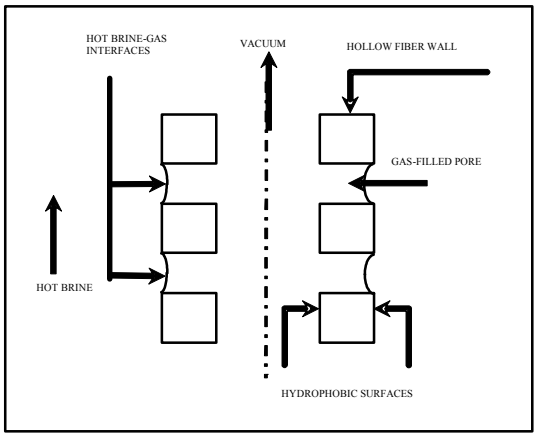

Fig. 1b. Conventional Vacuum Membrane distillation

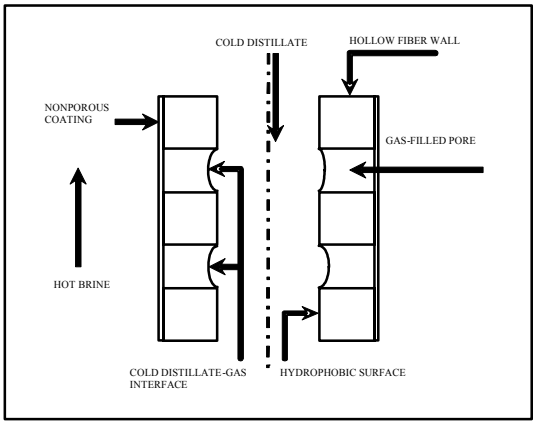

Fig. 1c. Suggested Direct Contact Membrane Distillation

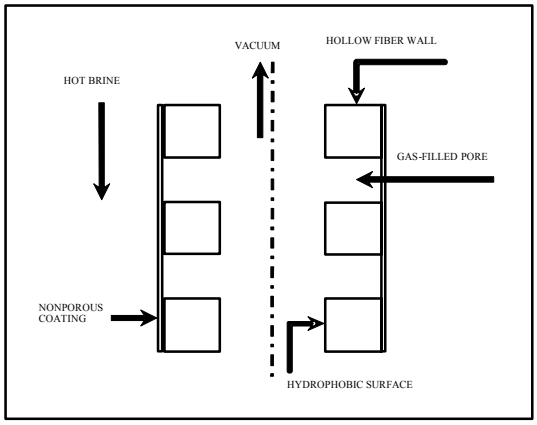

Fig.1d. Suggested Vacuum Membrane Distillation

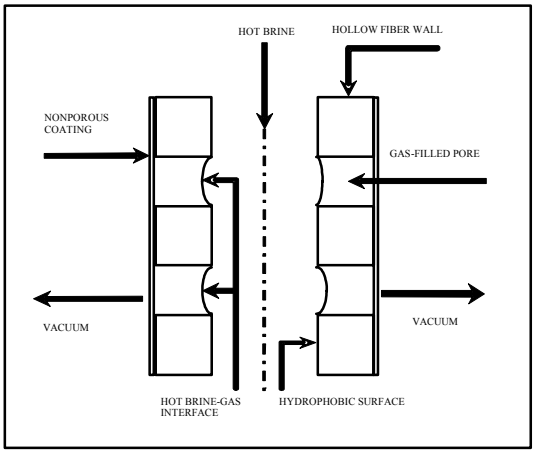

Fig. 1e. Vacuum Membrane Distillation with Hot Brine in Coated Fiber Lumen

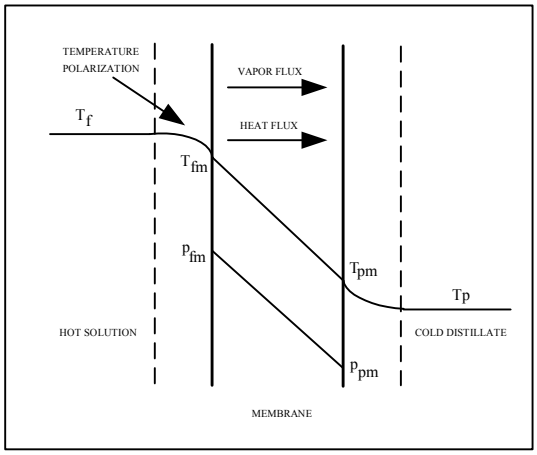

Fig. 1f. Temperature and Partial Pressure Profiles in Direct Contact Membrane Distillation

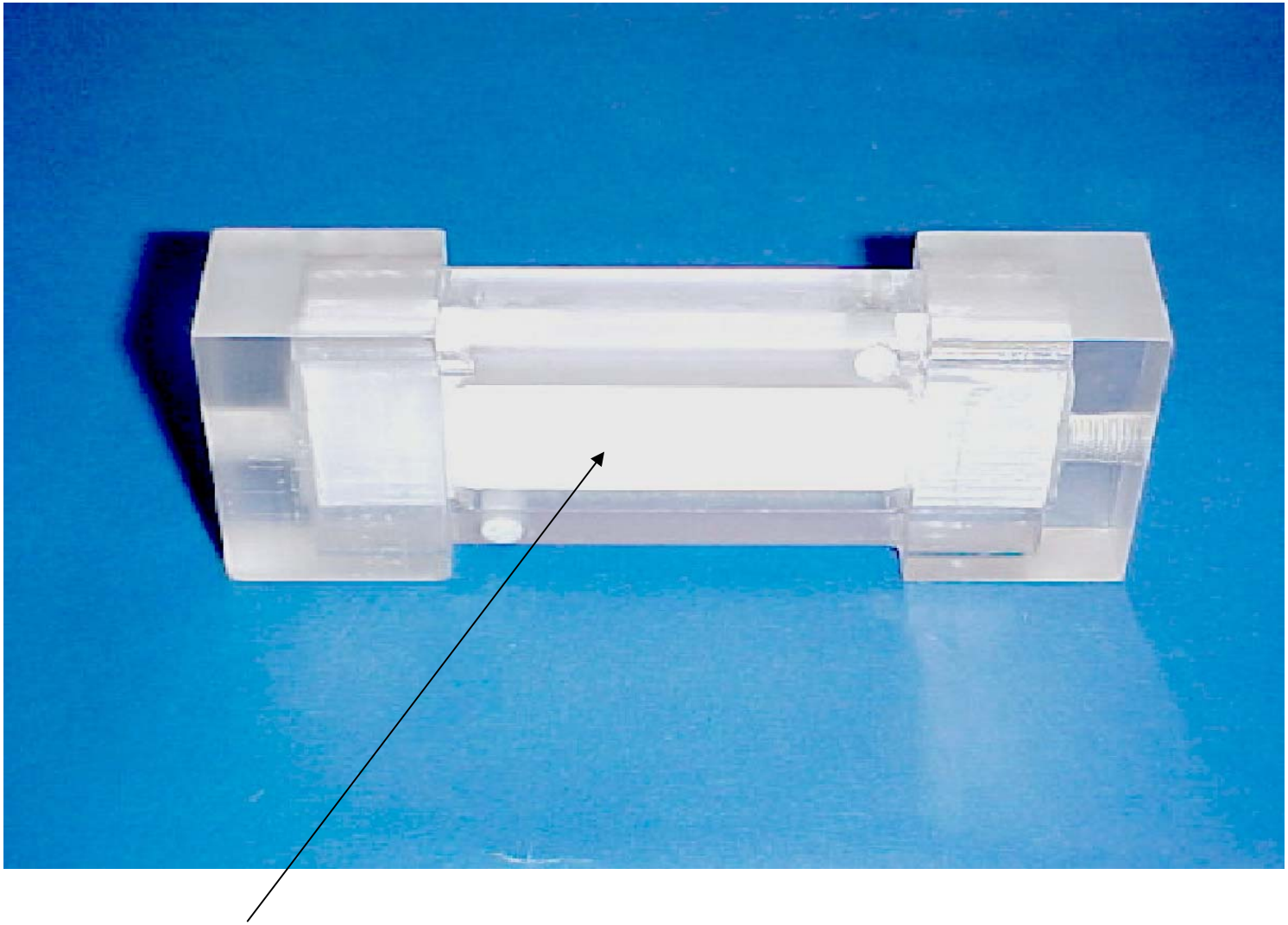

Figure 2a. Rectangular cross flow test module without face plates

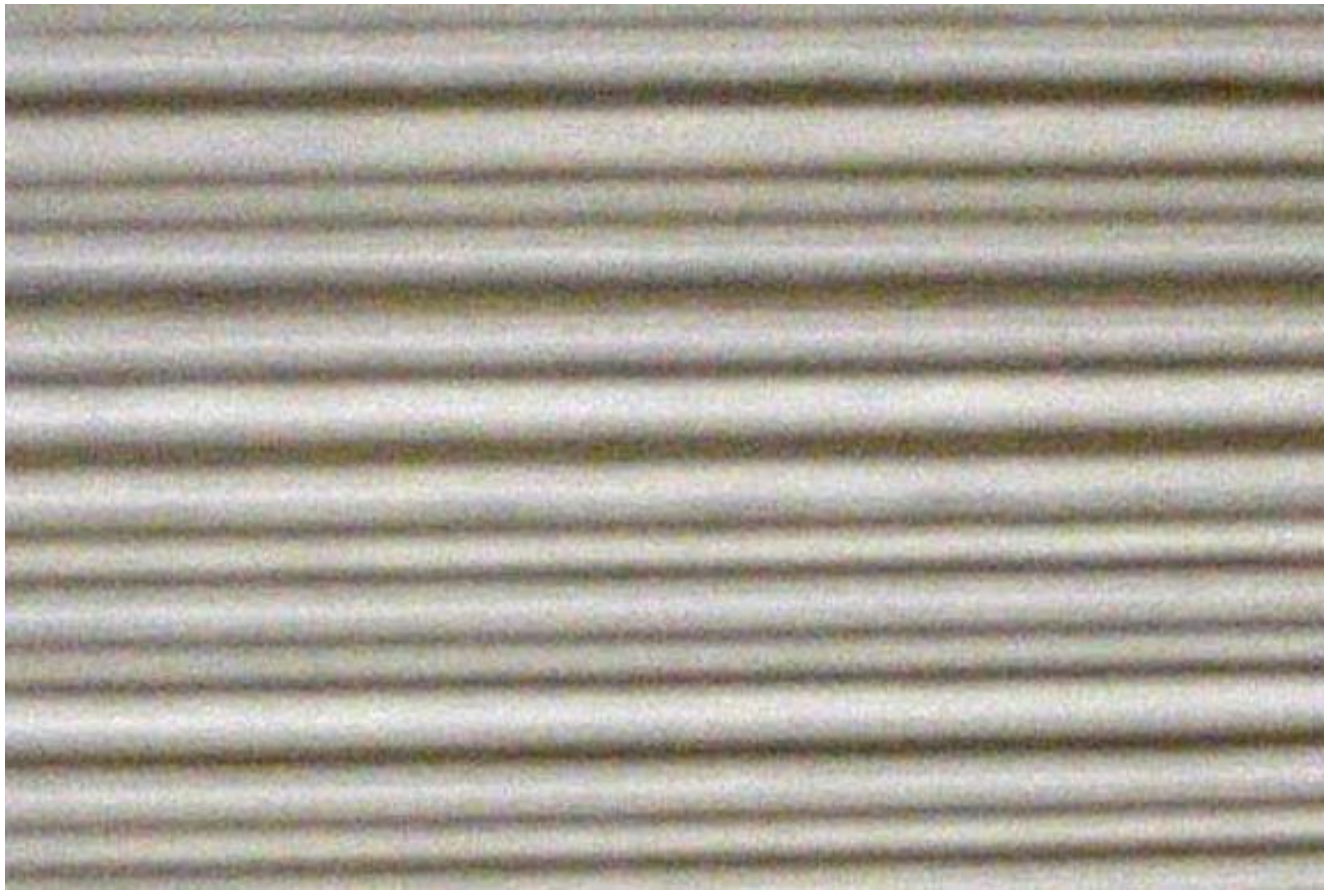

Figure 2b. Arrangement of the coated microporous hollow fibers in rectangular cross flow test module

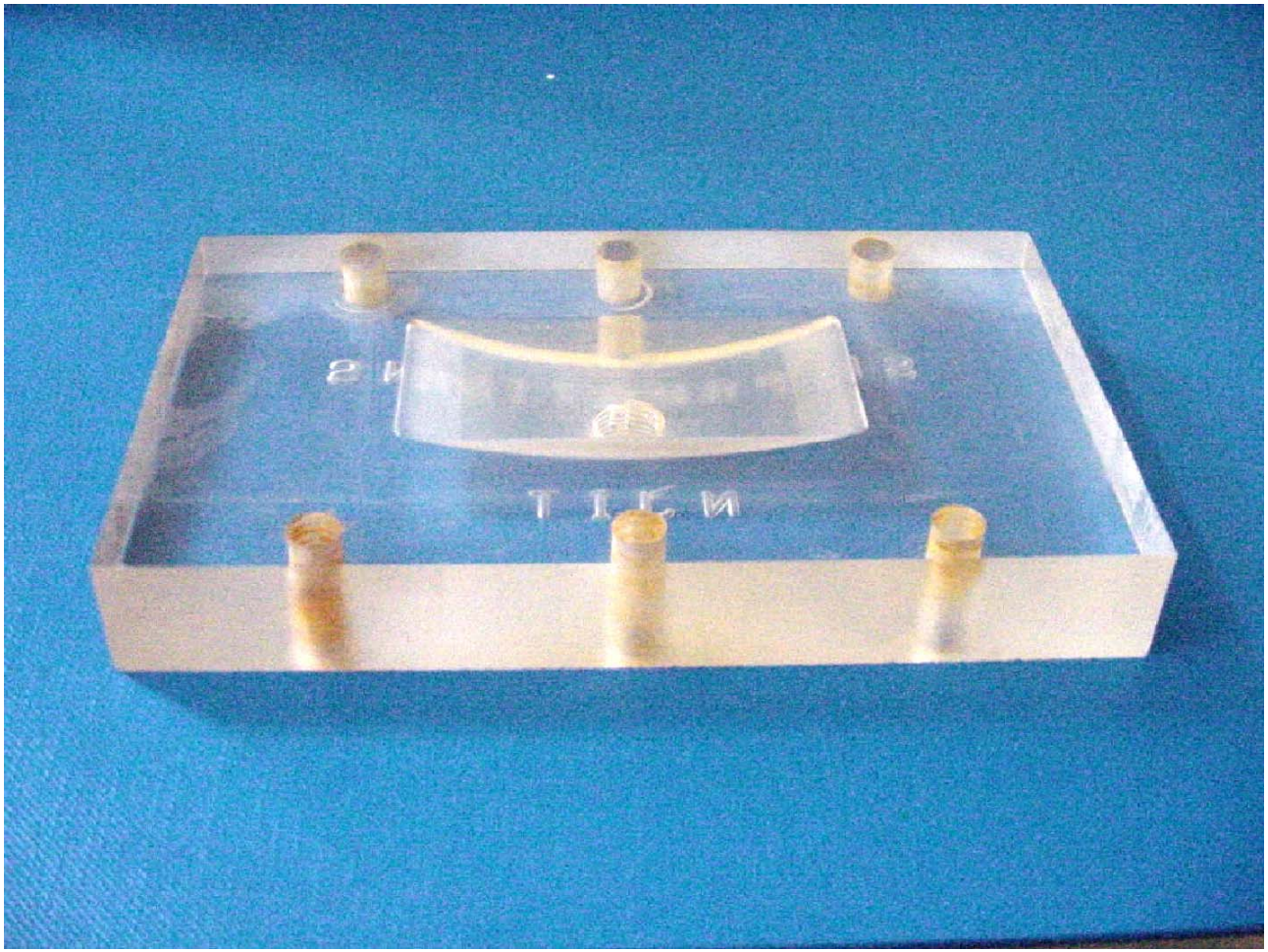

Figure 3. Face fabricated for rectangular cross flow module

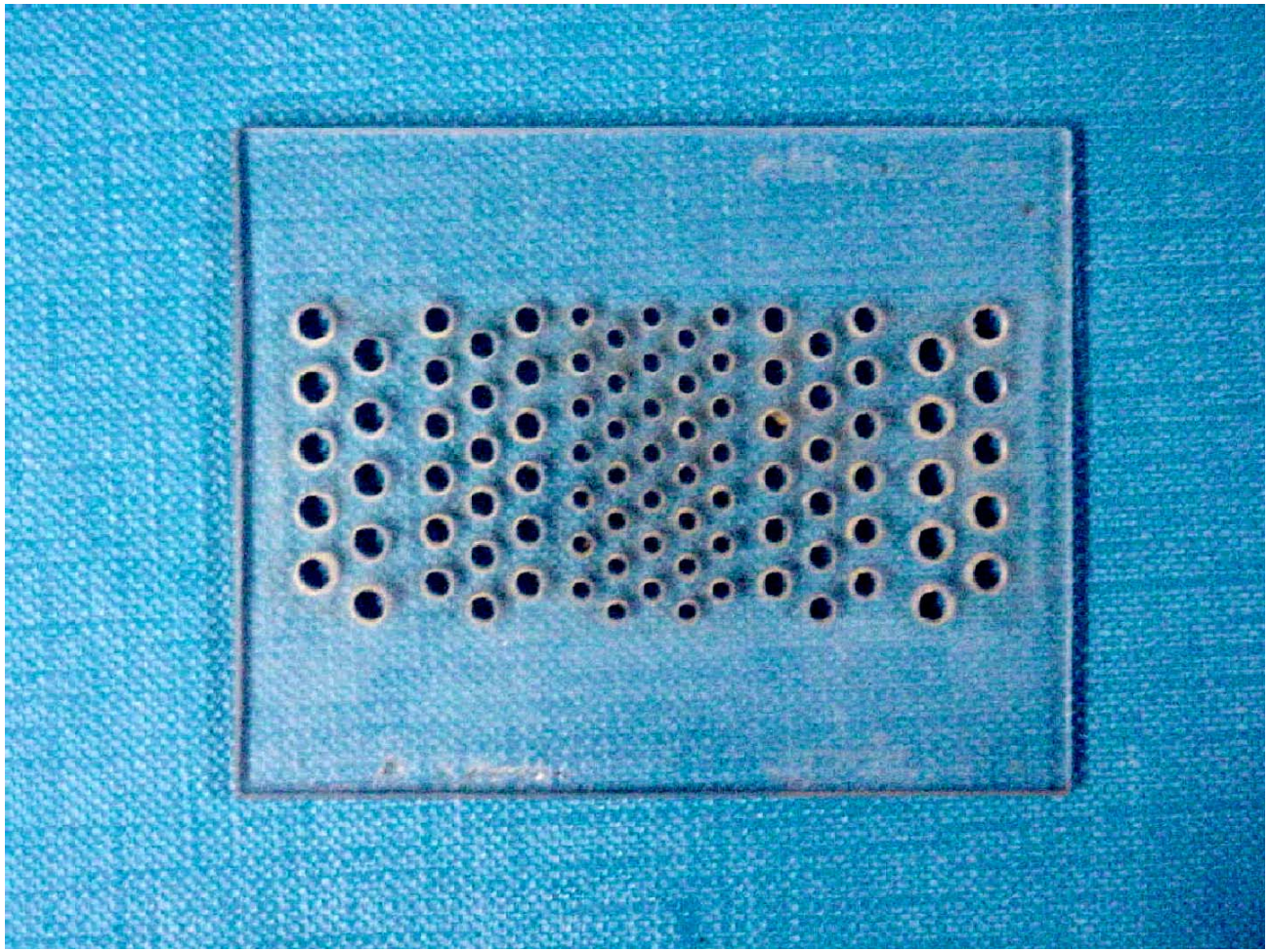

Figure 4. Face plate fabricated for rectangular cross flow module

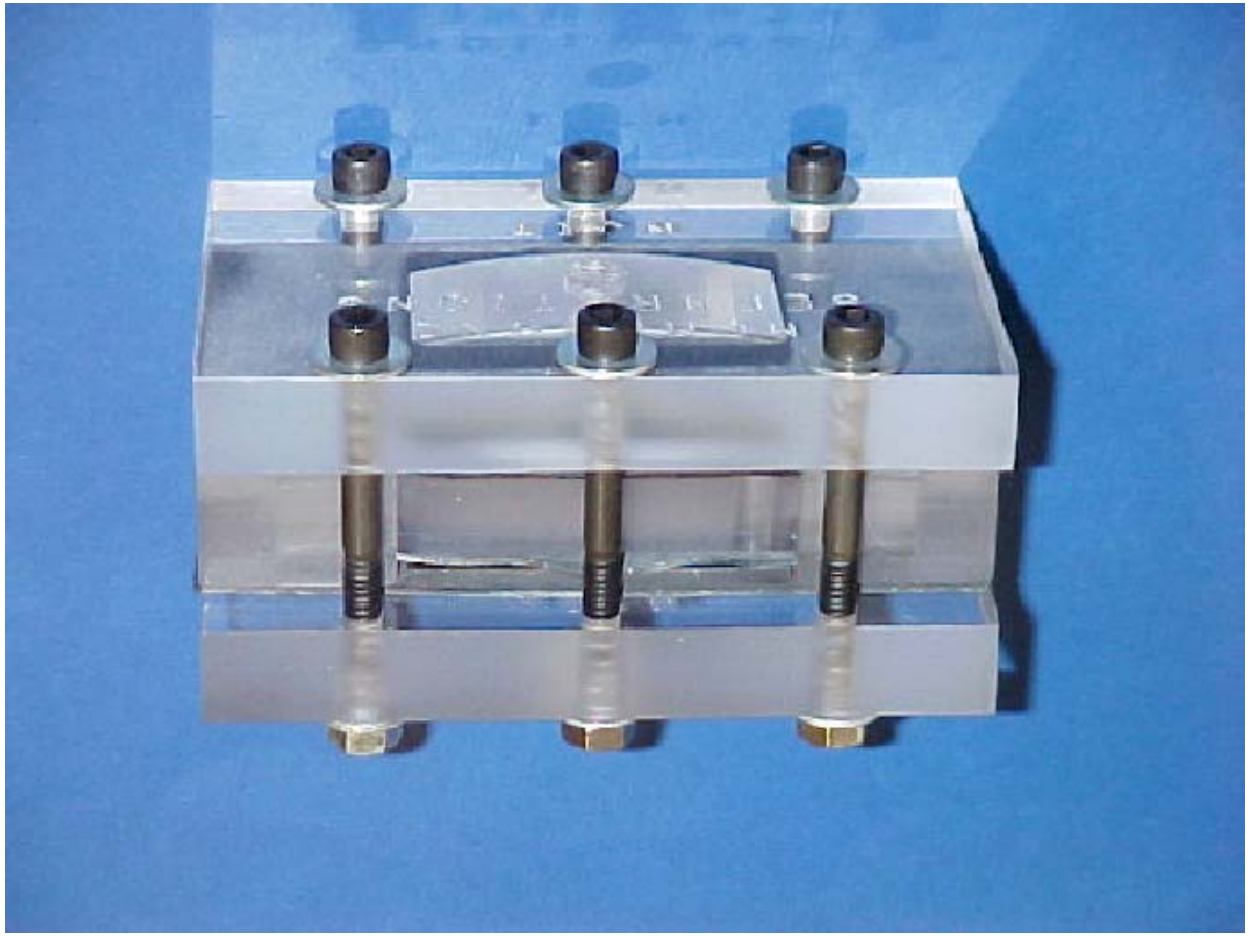

Figure 5. Rectangular cross flow test module with face boxes and plates and assembly

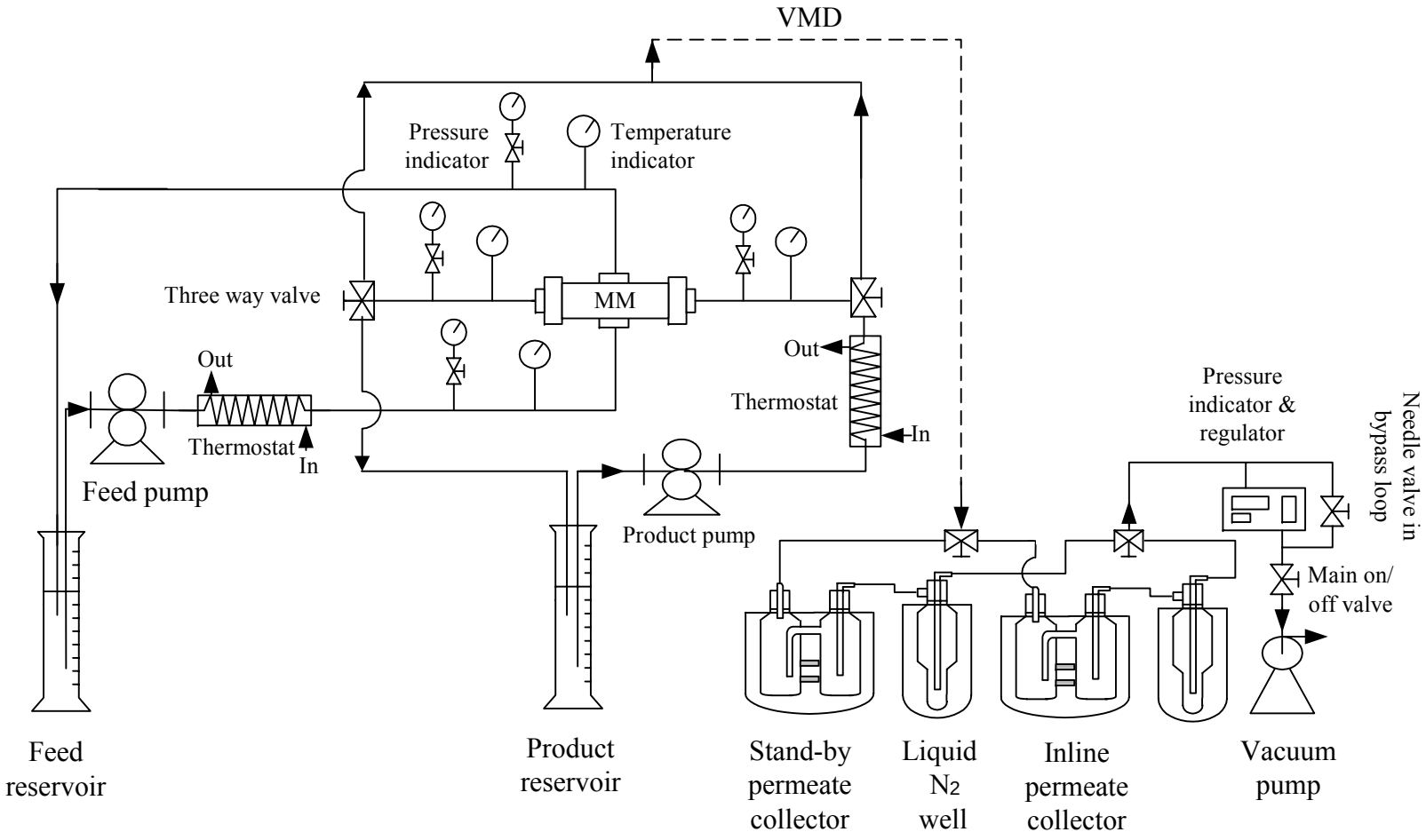

MM: Crossflow membrane moduel

Figure 6. Experimental setup for membrane distillation --- DCMD and VMD

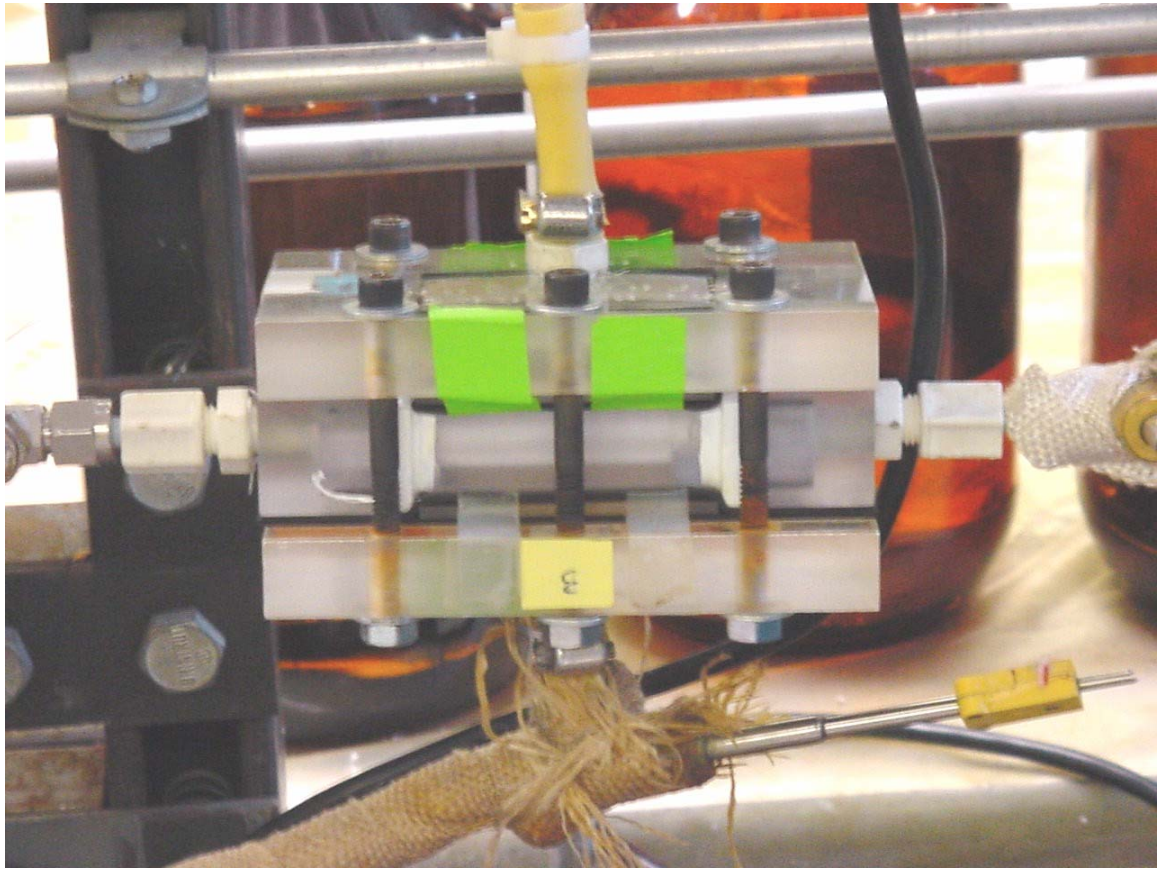

Figure 7. Photograph of the membrane module assembled in DCMD and VMD system

Figure 8. Photograph of the setup of Figure 6

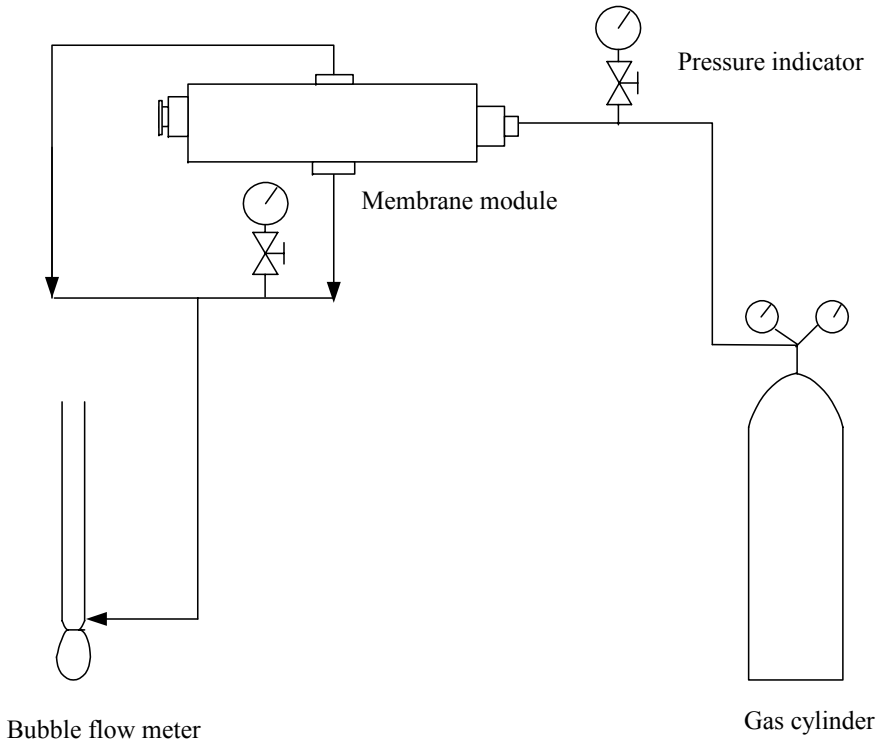

Figure 9. Experimental setup for membrane gas permeation measurement

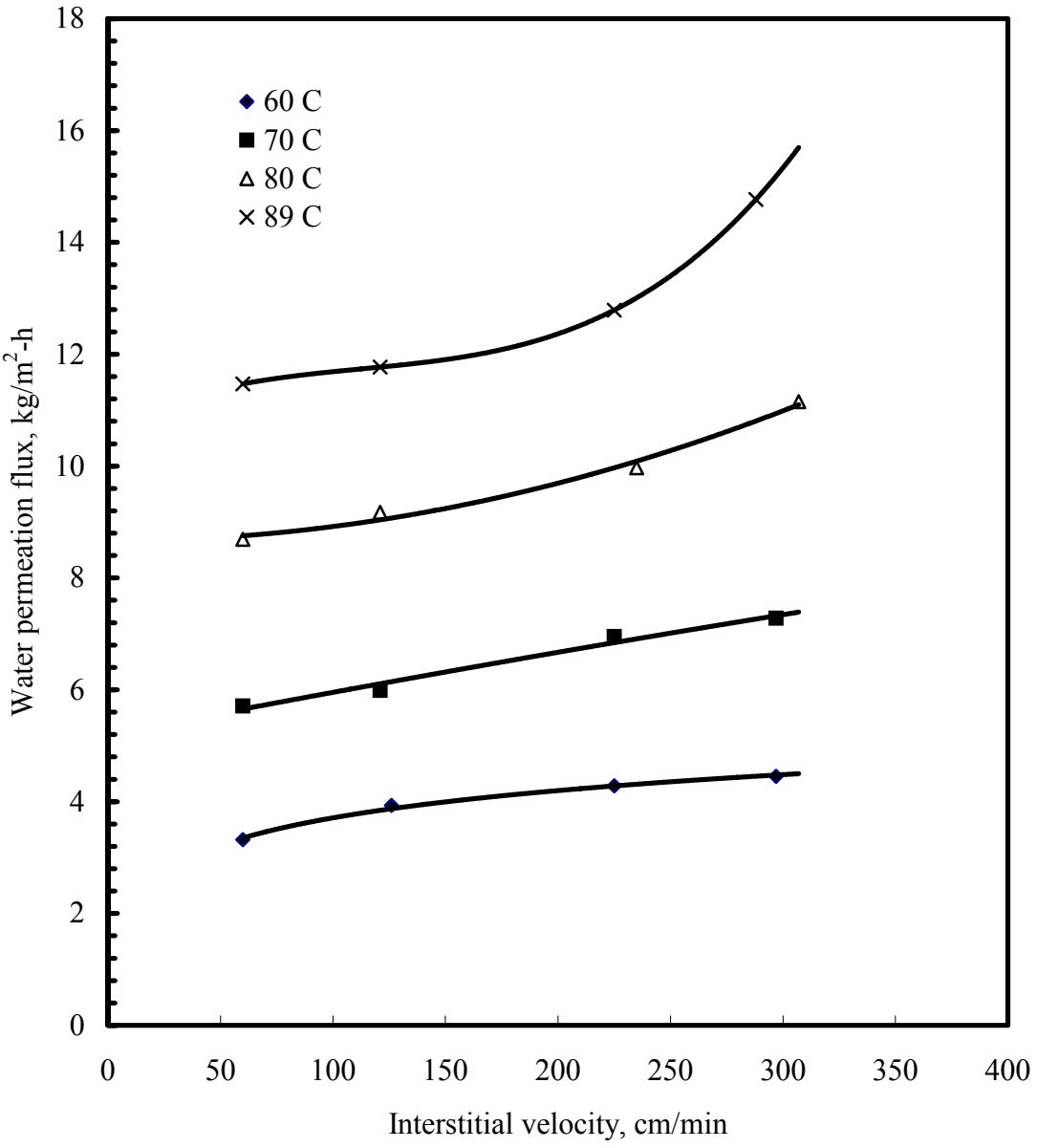

Figure 10. VMD: Variation of water vapor flux with interstitial velocity of hot brine (1% NaCl) flowing through the shell side (cross flow) at various temperatures (Module MXFR #6; vacuum at tube side: 63-66 cmHg)

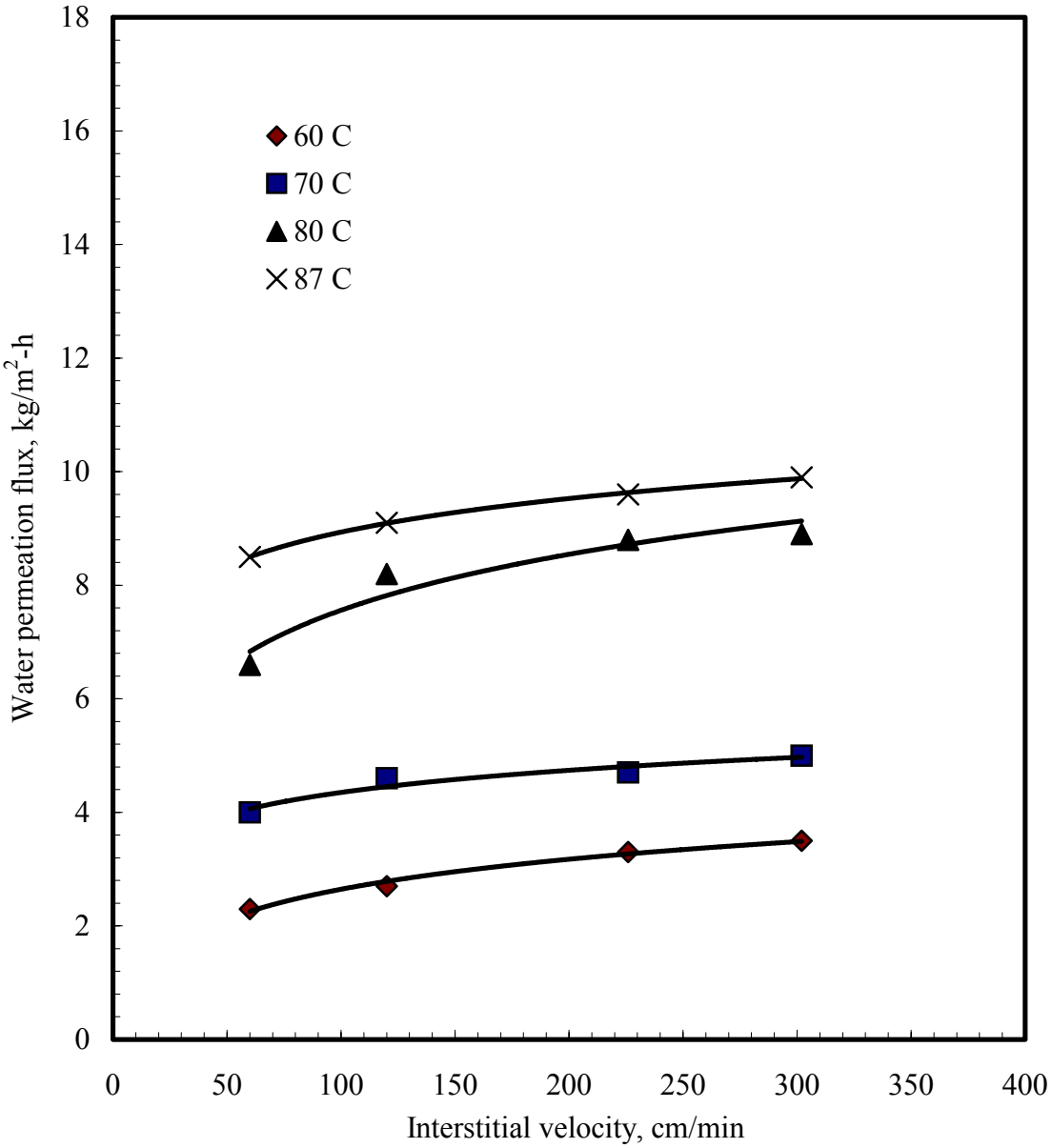

Figure 11. VMD: Variation of water vapor flux with interstitial velocity of hot brine (1% NaCl) flowing through the shell side (cross flow) at various temperatures (Module MXFR #7; vacuum at tube side: 63-66 cmHg)

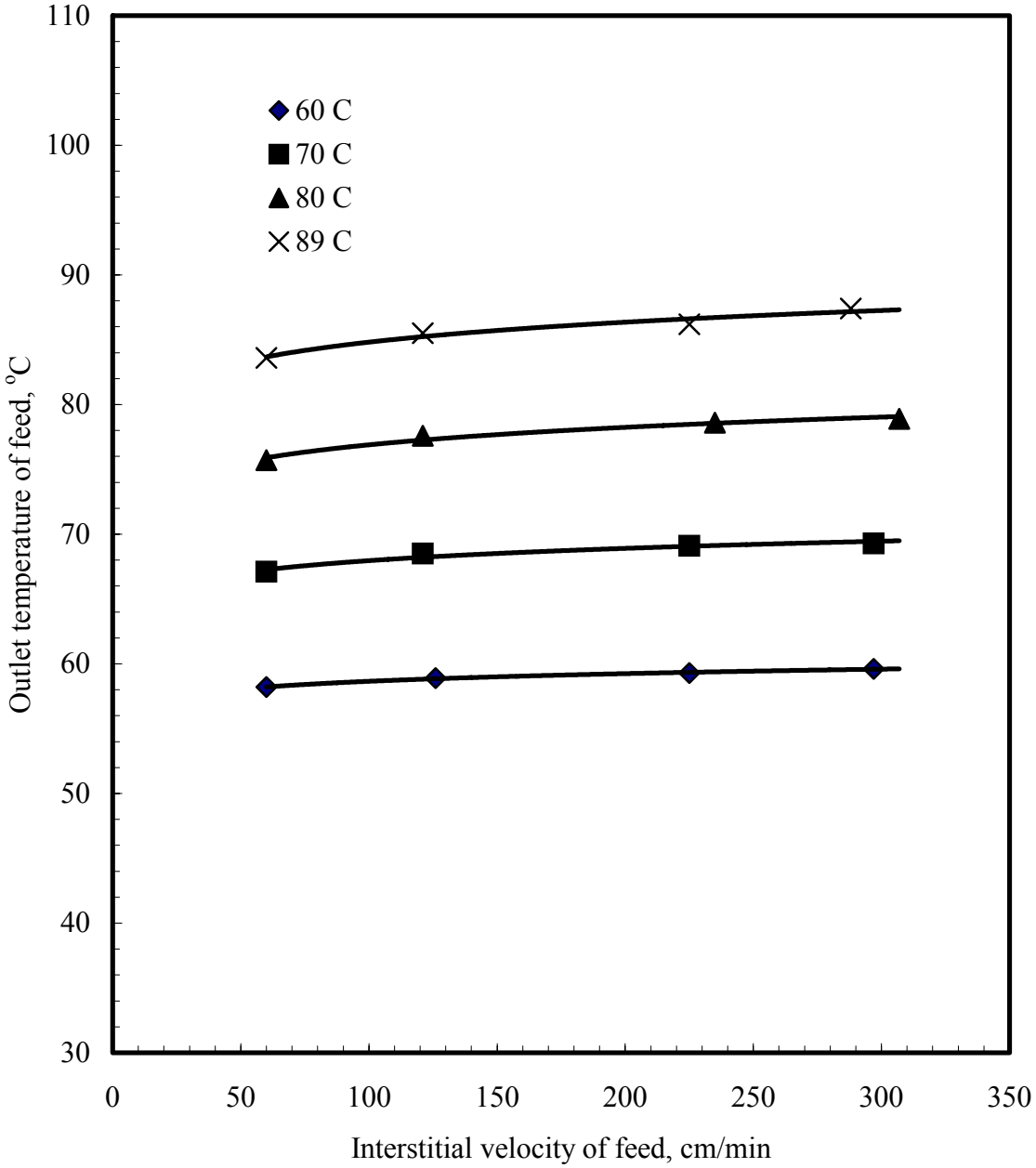

Figure 12. VMD: Variation of feed (1% brine) outlet temperature with feed interstitial velocity on the shell side of hollow fiber module at various inlet temperatures (MXFR #6; vacuum at tube side: 66-70 cmHg)

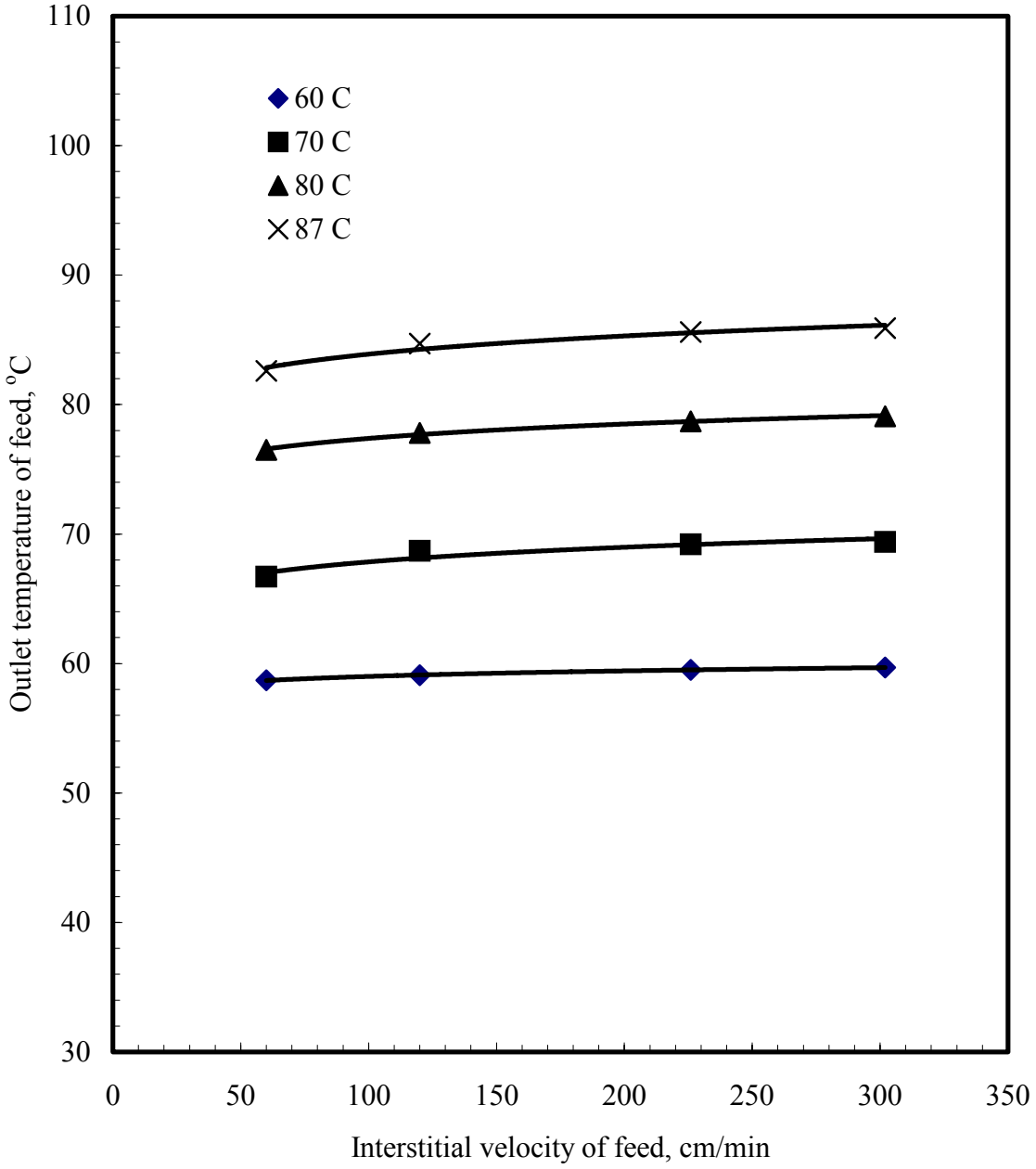

Figure 13. VMD: Variation of feed (1% brine) outlet temperature with feed interstitial velocity through shell side of hollow fiber module at various inlet temperatures (MXFR #7; vacuum at tube side: 63-66 cmHg)

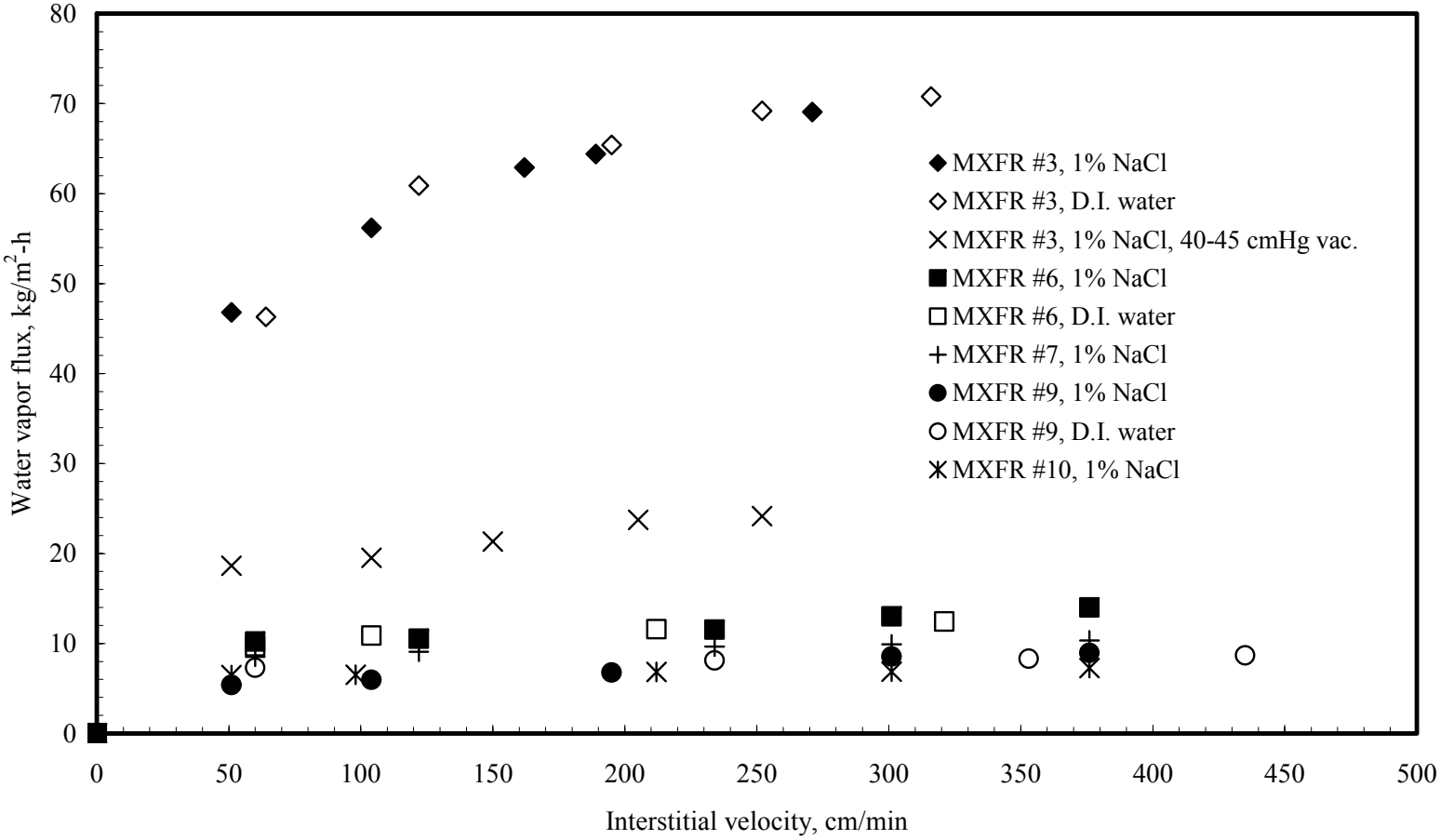

Figure 14. VMD: Variation of water vapor flux of modules MXFR #3, MXFR #6, MXFR #7, MXFR #9 and MXFR #10 with D.I. water or 1% brine as feed flowing through the shell side at 85 ^{o}C; tube side under a vacuum of 60-66 cmHg.

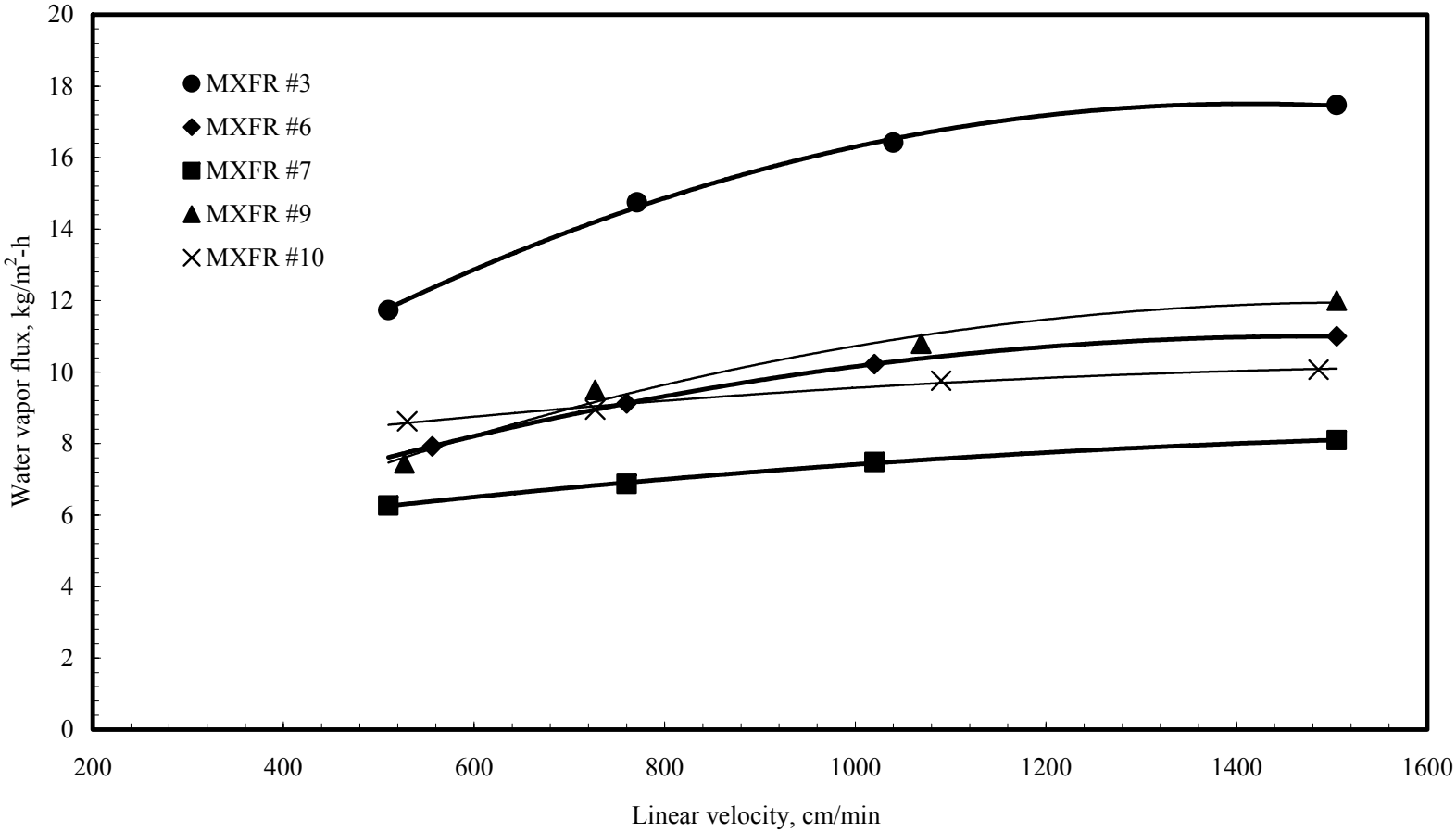

Figure 15. VMD: Variation of water vapor flux in modules MXFR #3, MXFR #6, MXFR #7, MXFR #9 and MXFR #10 with linear velocity of hot deionized water as feed flowing through the tube side at 85 ^{o}C (shell side: vacuum, 60-64 cmHg)

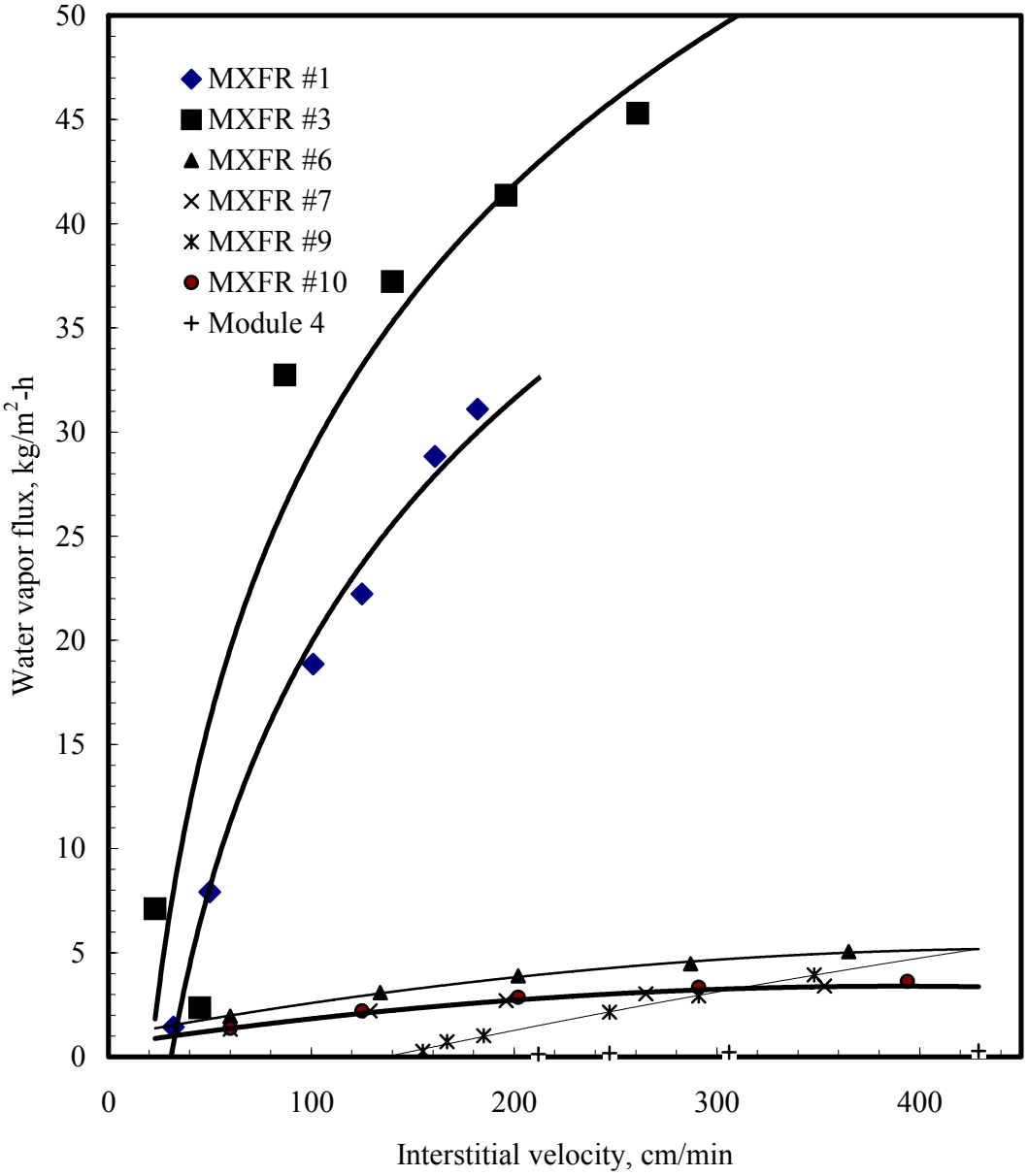

Figure 16. Comparison of the DCMD performances of all modules received from AMT, Inc. : variation of water vapor flux with velocity of hot brine (1% NaCl) as feed flowing through the shell side at 85 ^{o}C (tube side: D.I . water, 15-17 ^{o}C, linear velocity 760 cm/min)

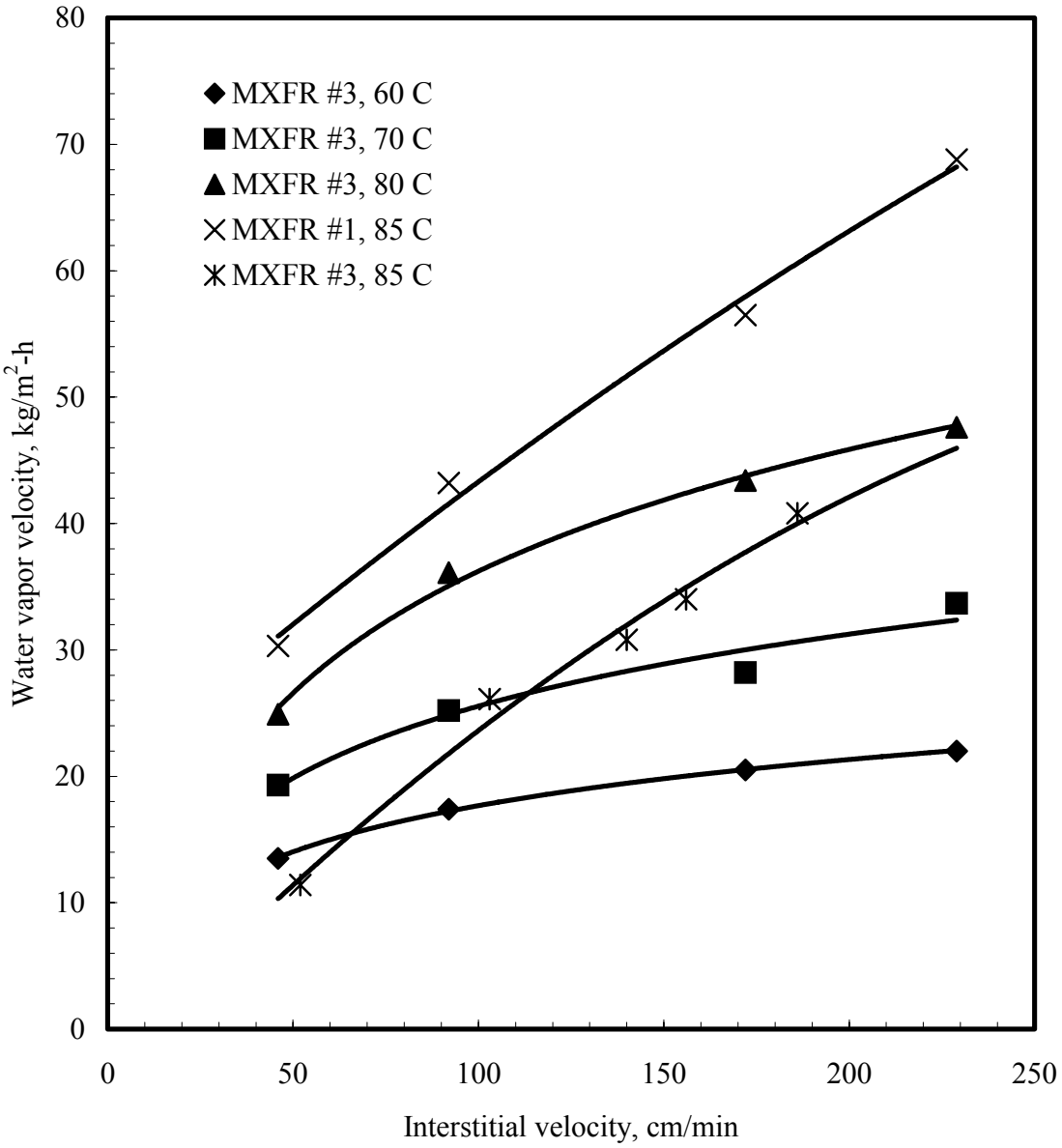

Figure 17. DCMD: Variation of water vapor flux with interstitial velocity of hot brine (1% NaCl) as feed flowing through the shell side (cross flow) at various temperatures (modules MXFR #3 and MXFR #1; tube side: 15-17 ^{o}C deionized water, average velocity 1660 cm/min)

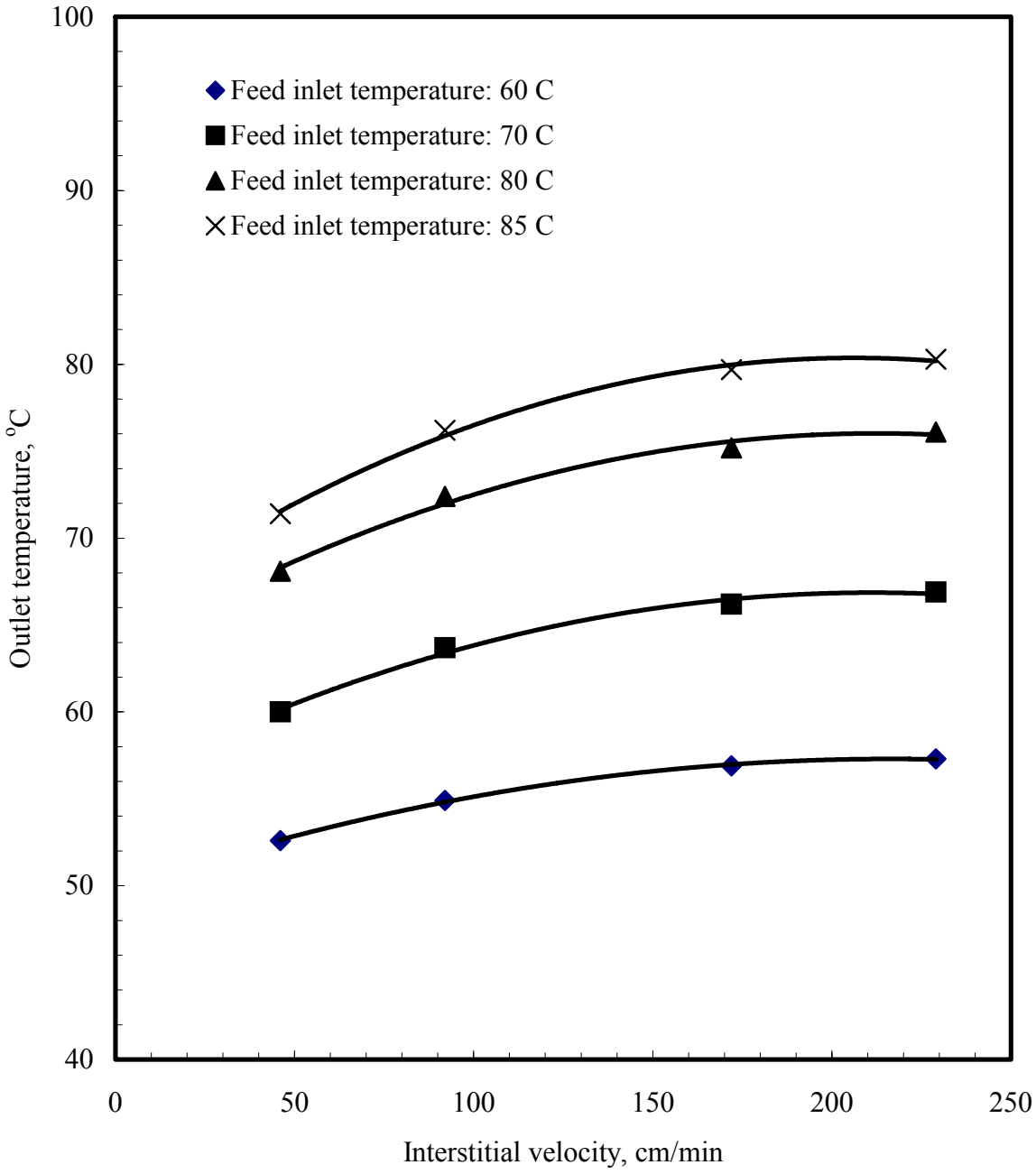

Figure 18. DCMD: Variation of feed outlet temperature with feed interstitial velocity through the shell side of hollow fiber module at various inlet temperatures (MXFR #3; Feed: 1 % NaCl; distillate: deionized water at 15-17 ^{o}C, 1660 cm/min of linear velocity)

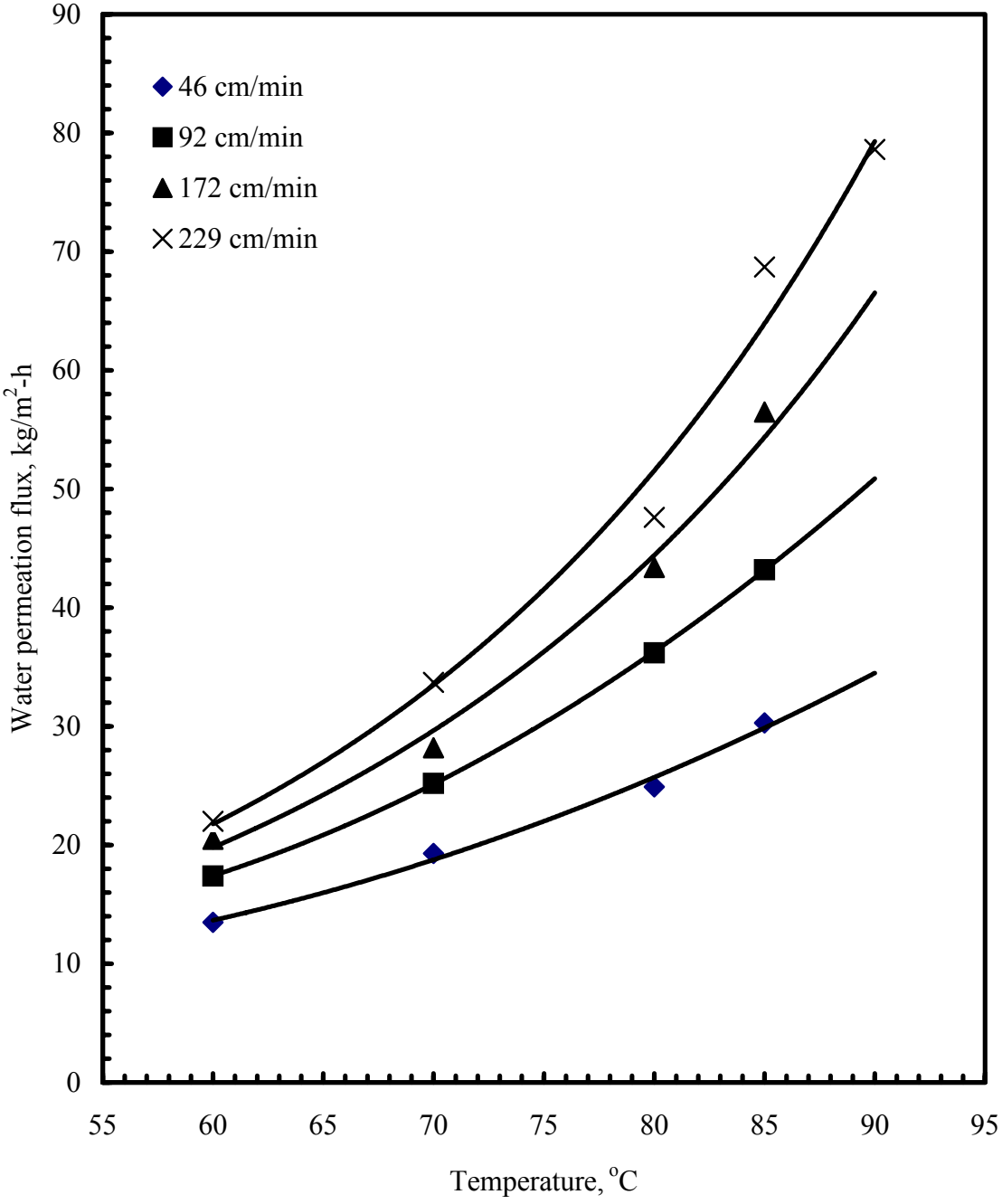

Figure 19. DCMD: Variation of water vapor flux with inlet temperature of hot brine (1% NaCl) as feed flowing through the shell side (cross flow) at various interstitial velocities (Module MXFR #3; tube side: 15-17 ^{o}C deionized water, velocity 1660 cm/min)

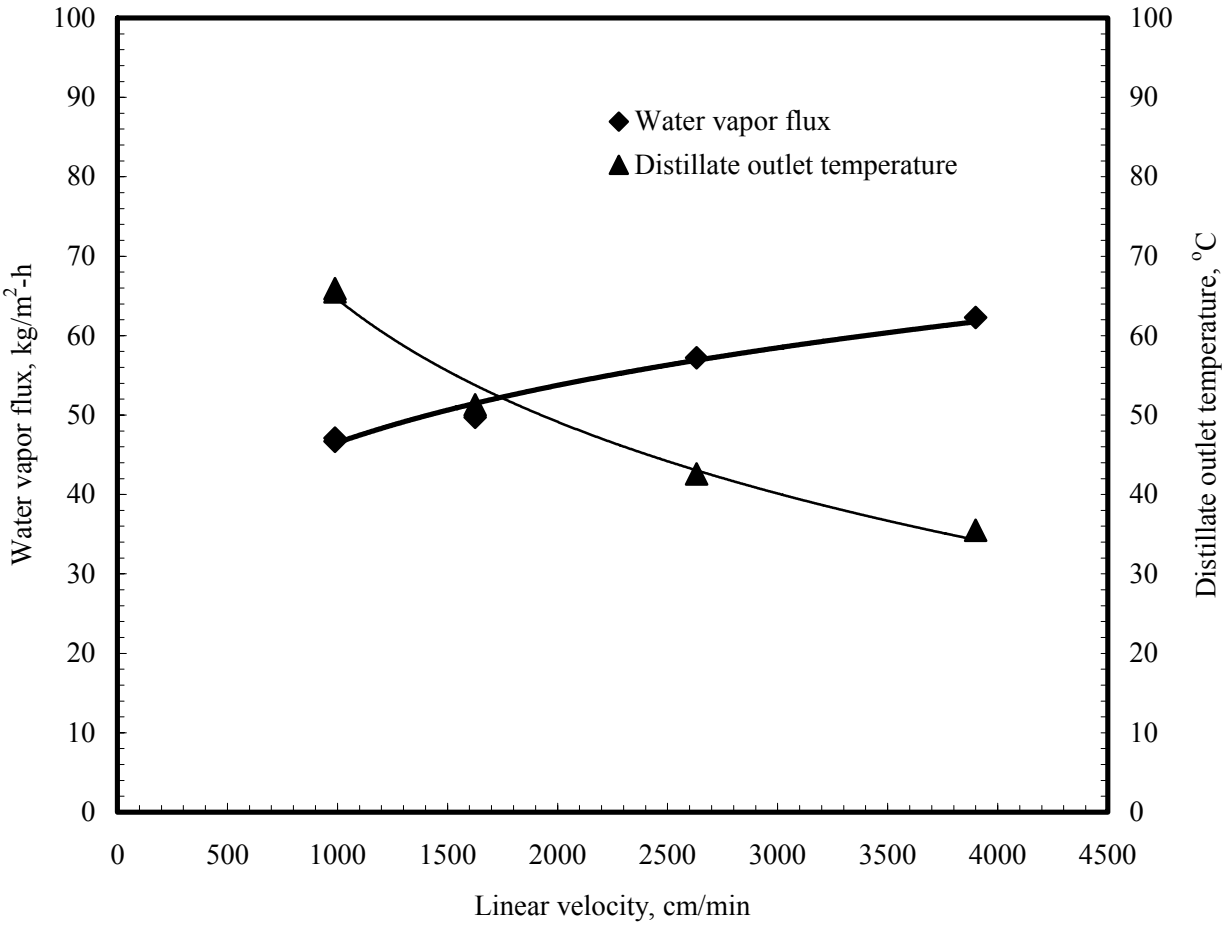

Figure 20. DCMD: Variation of water vapor flux and distillate outlet temperature with linear velocity of distillate (D.I. water) flowing through the tube side at entrance temperature of 15-23 ^{o}C (Module MXFR #3; shell side: brine solution (1% NaCl) at 85 ^{o}C, average velocity 229 cm/min)

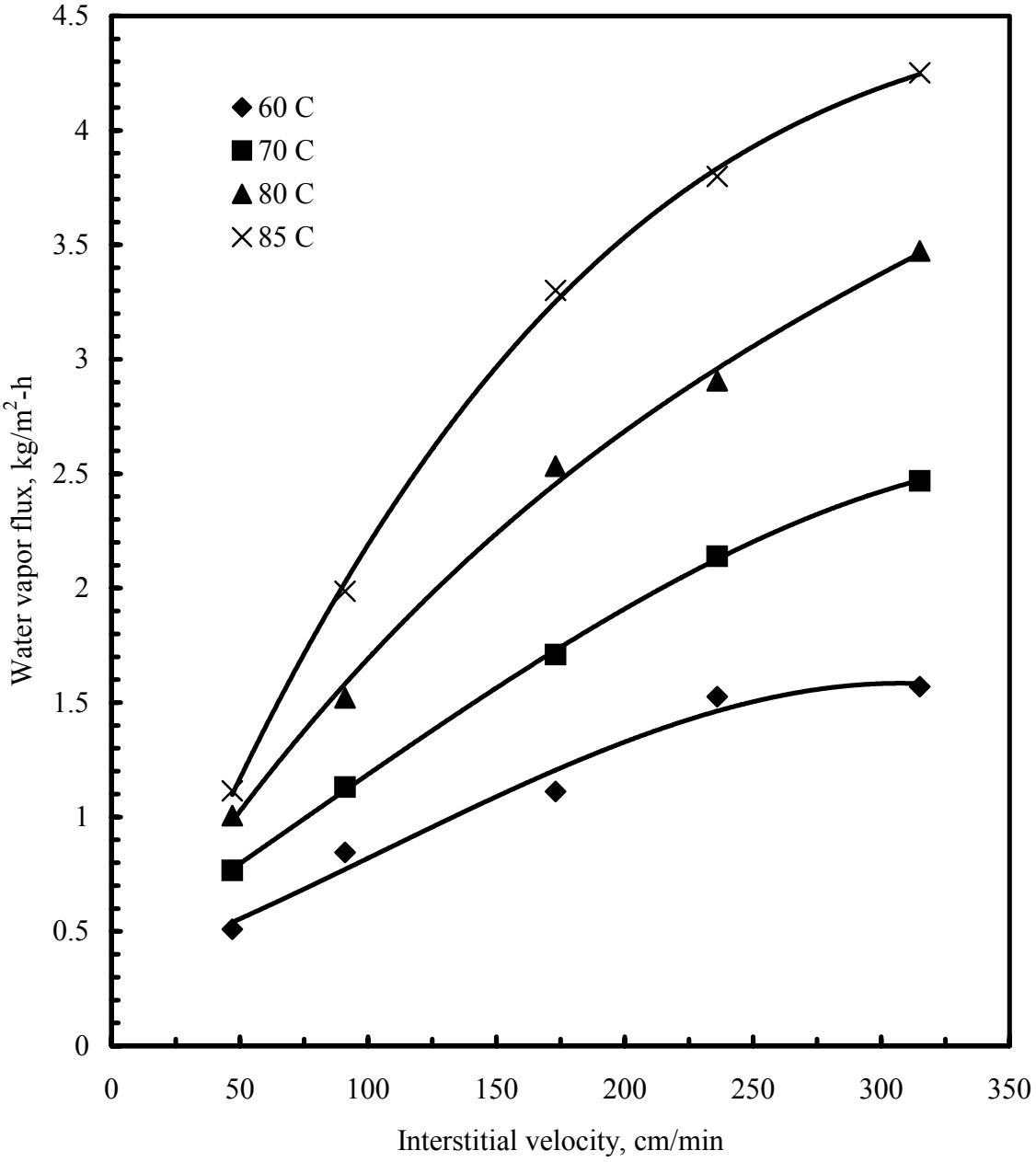

Figure 21. DCMD: Variation of water vapor flux with interstitial velocity of hot brine (1% NaCl) as feed flowing through the shell side (cross flow) at various temperatures (Module MXFR #9, tube side: 15-20 ^{o}C D.I. water, average linear velocity 1646 cm/min)

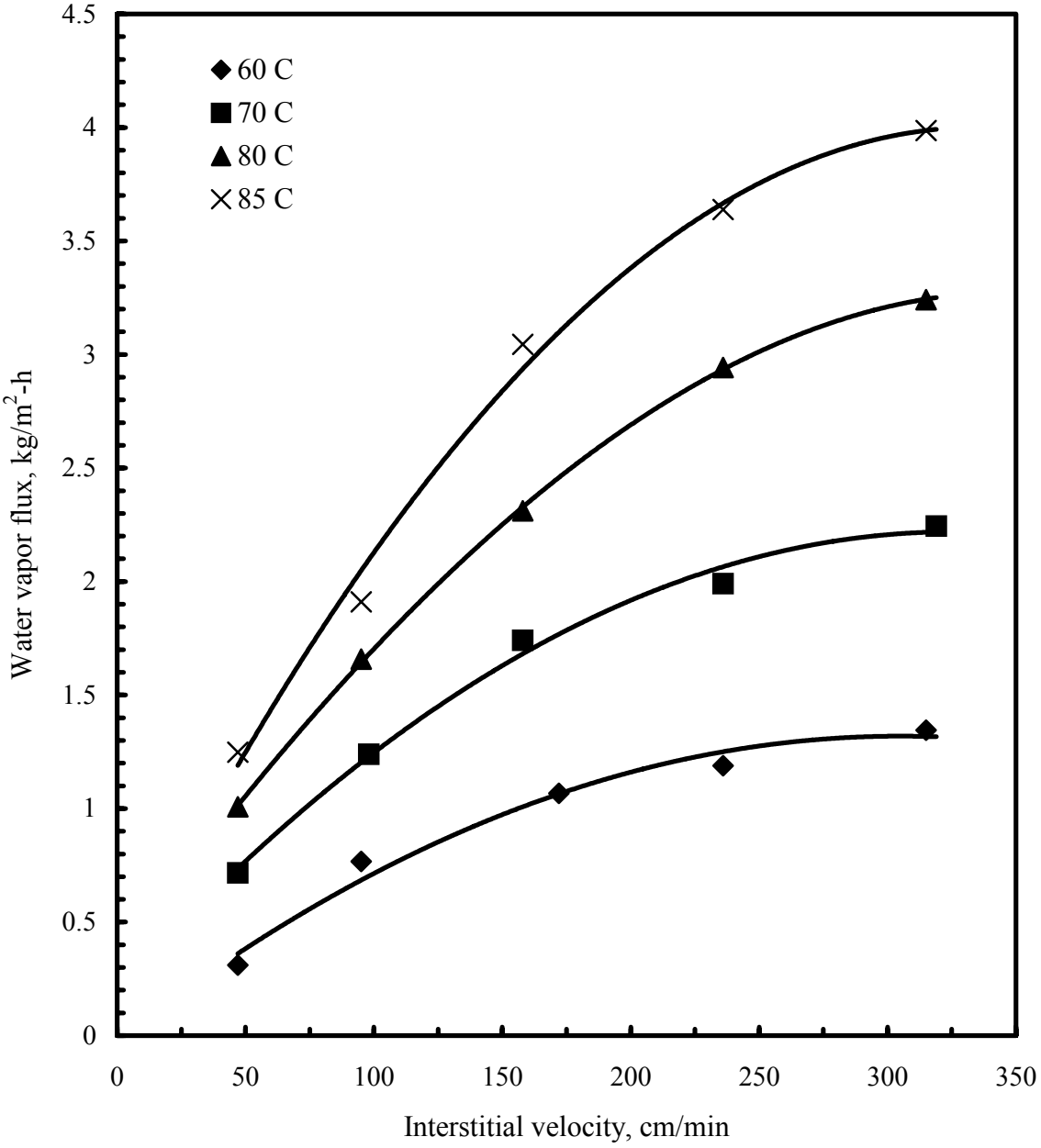

Figure 22. DCMD: Variation of water vapor flux with interstitial velocity of hot brine (1% NaCl) as feed flowing through the shell side (cross flow) at various temperatures (Module MXFR #10, tube side: D.I. water at 15-23 ^{o}C , average linear velocity 1643 cm/min)

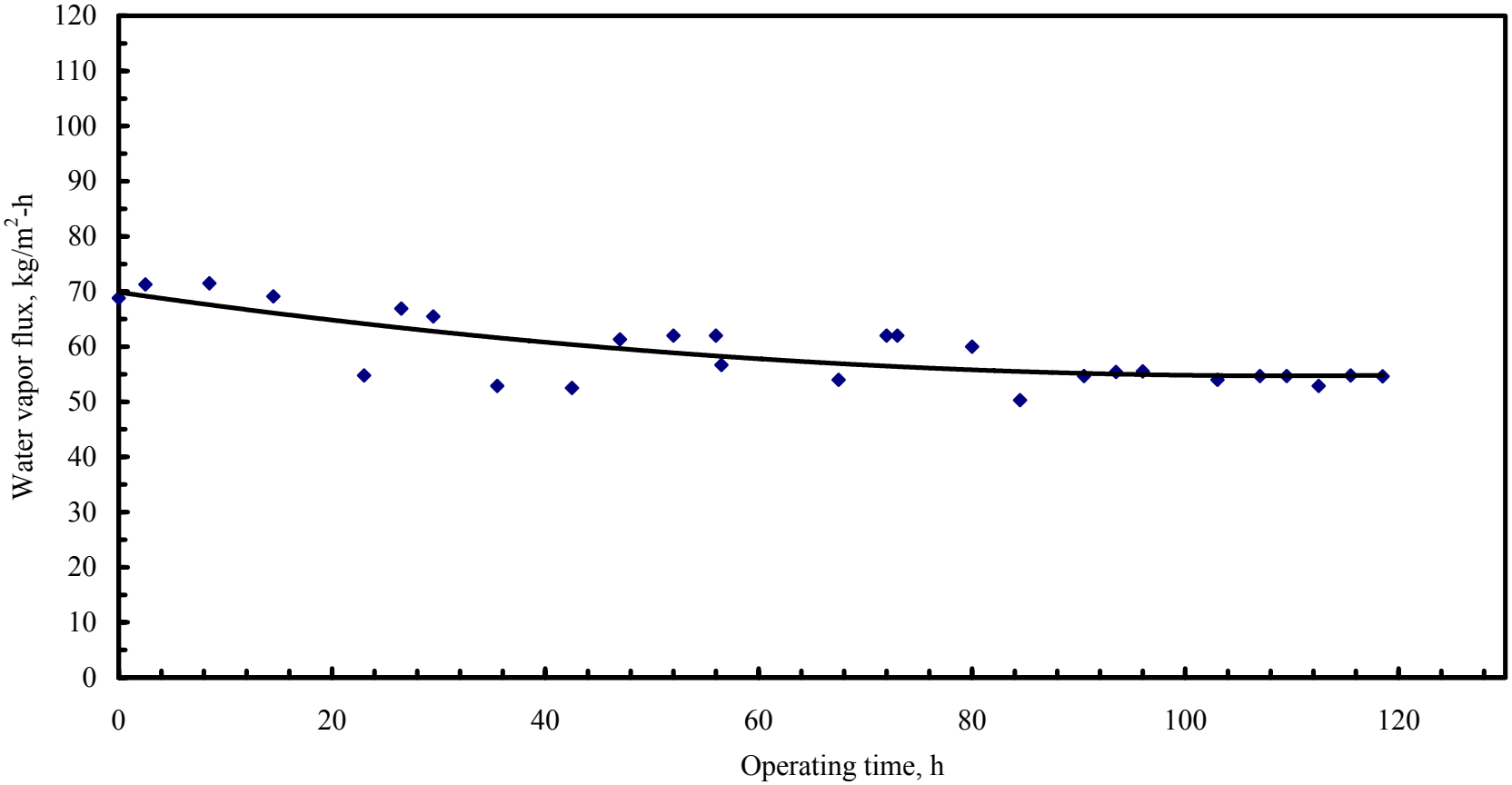

Figure 23. DCMD: Variation of water vapor flux with operating time for hot brine (1% NaCl) recirculating through the shell side with a velocity of 234 cm/min at 85.5 ^{o}C, and cold distillate water recirculating through tube side at a velocity of 1625 cm/min at 16 ^{o}C (Module MXFR #3)

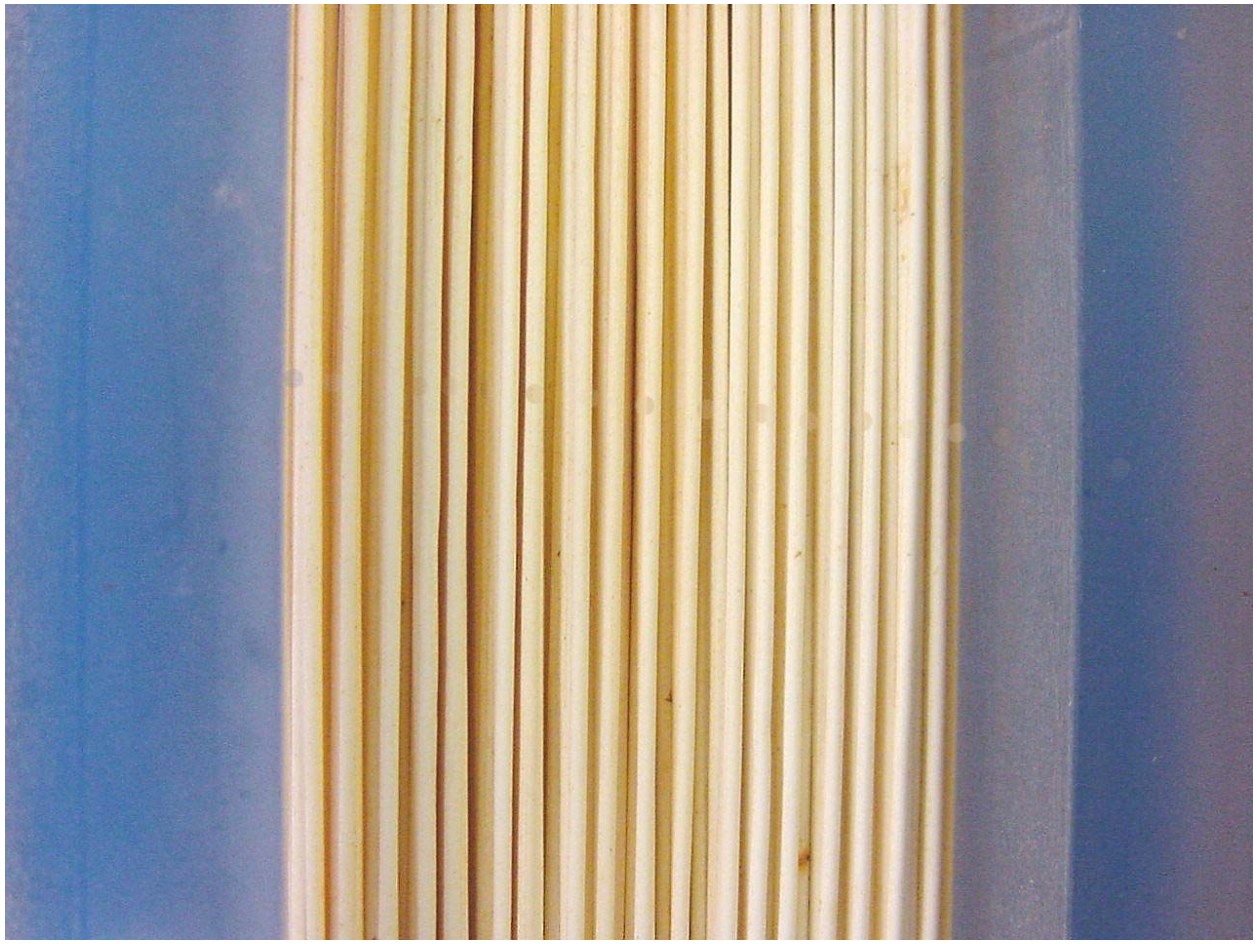

Figure 24. Status of hollow fibers in MXFR #3 after many runs spanning 400 hours (almost all fibers are separated from each other)

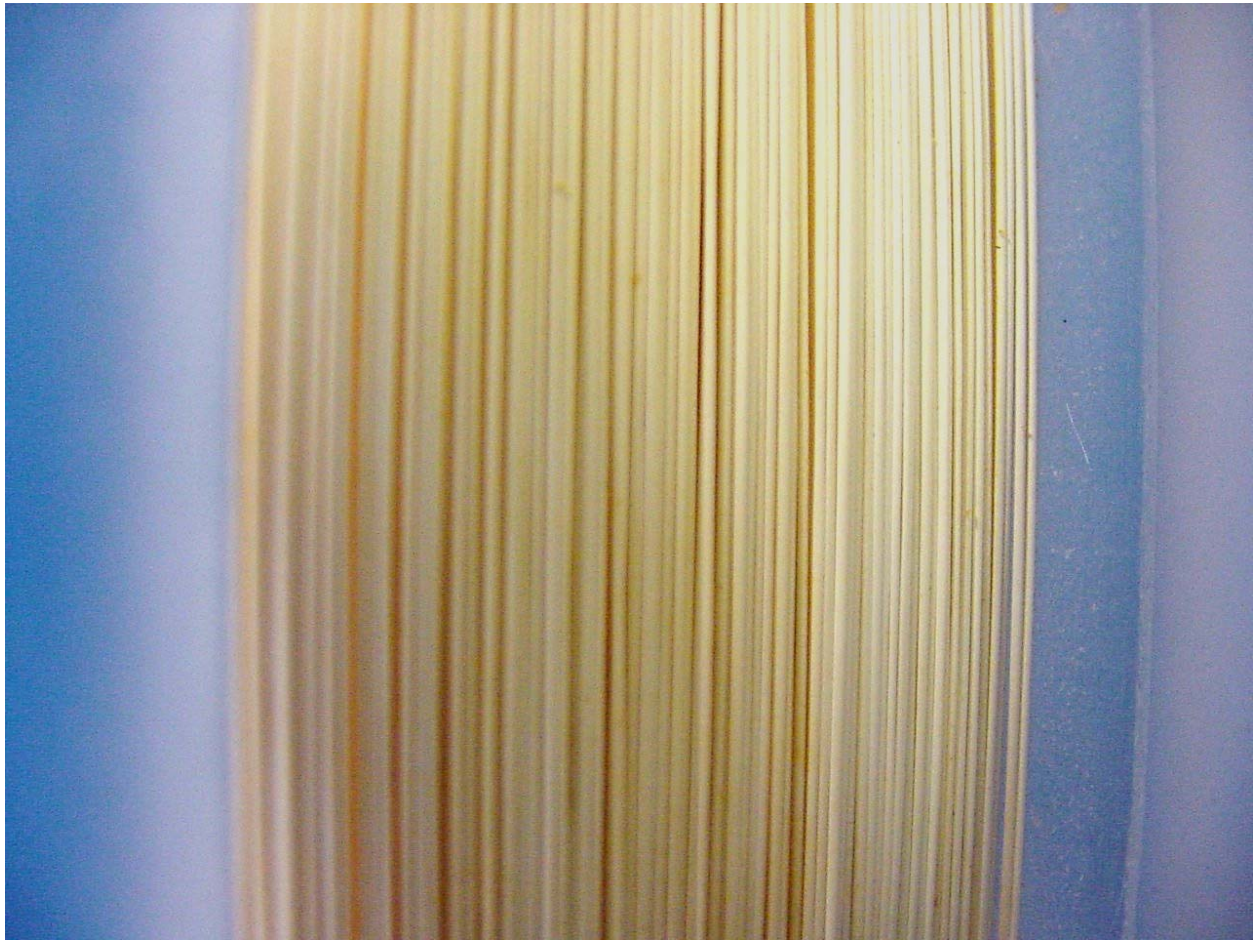

Figure 25. Status of hollow fibers in MXFR #7 during and after VMD or DCMD run (fibers appear to be sticking together)

Appendix

Data Tables

Table A1. Experimental data used in Figure 10. VMD: Variation of water vapor flux with interstitial velocity of hot brine (1% NaCl) flowing through the shell side (cross flow) at various temperatures (Module MXFR #6; vacuum at tube side: 63-66 cmHg)

Interstitial Velocity, cm/min	Feed inlet temperature, °C			
	60	70	80	89
	Water vapor flux, kg/m^2-h			
60	3.32	5.71	8.69	11.47
121		5.99	9.17	11.77
126	3.93			
225	4.28	6.95		12.79
235			9.97	
288				14.77
297	4.45	7.28		
307			11.15	

Table A2. Experimental data used in Figure 11. VMD: Variation of water vapor flux with interstitial velocity of hot brine (1% NaCl) flowing through the shell side (cross flow) at various temperatures (Module MXFR #7; vacuum at tube side: 63-66 cmHg)

Interstitial velocity (cm/min)	Feed inlet temperature, °C			
	60	70	80	87
	Water vapor flux, kg/m^2-h			
60	2.3	4	6.6	9.3
120	2.7	4.6	8.2	9.6
226	3.3	4.7	8.8	10
302	3.5	5	8.9	10.5

Table A3. Experimental data used in Figure 12. VMD: Variation of feed outlet temperature with feed (1% brine) interstitial velocity on the shell side of hollow fiber module at various inlet temperatures (MXFR #6; vacuum at tube side: 66-70 cmHg)

Interstitial Velocity, cm/min	Feed inlet temperature, °C			
	60	70	80	89
	Feed outlet temperature, °C			
60	58.2	67.1	75.7	83.6
121		68.5	77.6	85.5
126	58.9			
225	59.3	69.1		86.2
235			78.6	
288				87.4
297	59.6	69.3		
307			78.9	

Table A4. Experimental data used in Figure 13. VMD: Variation of feed outlet temperature with feed (1% brine) interstitial velocity through shell side of hollow fiber module at various inlet temperatures (MXFR #7; vacuum at tube side: 63-66 cmHg)

Interstitial velocity, (cm/min)	Feed inlet temperature, °C			
	60	70	80	87
	Feed outlet temperature, °C			
60	58.7	66.7	76.5	82.6
120	59.1	68.7	77.8	84.7
226	59.5	69.2	78.7	85.6
302	59.7	69.4	79.1	85.9

Table A5. Experimental data used in Figure 14. VMD: Variation of water vapor flux of modules MXFR #3, MXFR #6, MXFR #7, MXFR #9 and MXFR #10 with D.I. water or 1% brine as feeds flowing through the shell side at 85 °C respectively ; tube side at vacuum of 60-66 cmHg.

Interstitial Velocity, cm/min	Membrane module								
	MXFR #3	MXFR #3	MXFR #3*	MXFR #6	MXFR #6	MXFR #7	MXFR #9	MXFR #9	MXFR #10
	Feed solution								
	1% NaCl	D.I. water	1% NaCl	1% NaCl	D.I. water	1% NaCl	1% NaCl	D.I. water	1% NaCl
	Water vapor flux, kg/m^2-h								
51	46.790		18.624				5.397		6.470
60				10.205	9.666	8.517		7.306	
64		46.291							
98									6.526
104	56.200		19.505		10.875		5.944		
122		60.908		10.522		9.095			
150			21.345						
162	62.888								
195	64.400	65.400					6.761		
205			23.753						
212					11.586				6.817
234				11.512		9.637		8.110	
252		69.200	24.149						
271	69.076								
301				12.990		9.901	8.545		6.859
316		70.800							
321					12.450				
353								8.305	
376				14.000		10.335	8.959		7.255
435								8.663	

* Tube side at vacuum of 40-45 cm Hg.

Table A6. Experimental data used in Figure 15. VMD: Variation of water vapor flux in modules MXFR #3, MXFR #6, MXFR #7, MXFR #9 and MXFR #10 with velocity of hot deionized water as feed flowing through the tube side at 85 °C (shell side: vacuum, 60-64 cmHg)

Linear velocity, cm/min	Water vapor flux, kg/m^2-h				
	MXFR #3	MXFR #6	MXFR #7	MXFR #9	MXFR #10
510	11.731		6.269		
527				7.444	
530					8.625
556		7.925			
727				9.500	8.949
760		9.121	6.870		
771	14.748				
1020		10.226	7.481		
1040	16.418				
1069				10.800	
1090					9.759
1486					10.070
1505	17.469	11.003	8.096	12.001	

Table A7. Experimental data used in Figure 16. Comparison of the DCMD performances of all modules (received from AMT, Inc.): variation of water vapor flux with velocity of hot brine (1% NaCl) as feed flowing through the shell side at 85 °C (tube side: D.I . water, 15-17 °C, linear velocity 760 cm/min)

Interstitial velocity, cm/min	Water vapor flux, kg/m^2-h						
	MXFR#1	MXFR#3	MXFR#6	MXFR#7	MXFR#9	MXFR#10	Module4
23		7.108					
32	1.436						
45		23.491					
50	7.917						
60			1.95	1.323		1.37	
87		32.744					
101	18.865						
125	22.23					2.205	
129				2.213			
134			3.092				
140		37.223					
155					0.263		
161	28.826						
167					0.727		
185					1.009		
182	31.1						
196		41.362		2.695			
202			3.888			2.869	
212							0.131
247					2.143		0.175
261		45.3					
265				3.031			
287			4.468				
291					2.925	3.333	
306							0.22
348					3.939		
353				3.4			
365			5.05				
394						3.623	
429							0.283

Table A8. Experimental data used in Figure 17. DCMD: Variation of water vapor flux with interstitial velocity of hot brine solution (1% NaCl) as feed flowing through the shell side (crossflow) at various temperatures (modules MXFR #3 and MXFR #1; tube side: 15-17 °C deionized water, average linear velocity 1660 cm/min)

Interstitial velocity, (cm/min)	Feed inlet temperature, °C				
	60 (MXFR #3)	70 (MXFR #3)	80 (MXFR #3)	85 (MXFR #3)	85 (MXFR #1)
	Water vapor flux, kg/m^2-h				
46	13.5	19.3	24.9	30.3	
52					11.4
92	17.4	25.2	36.1	43.2	
103					26.1
140					30.8
156					34
172	20.5	28.2	43.4	56.5	
186					40.8
229	22	33.7	47.6	68.8	

Table A9. Experimental data used in Figure 18. DCMD: Variation of feed outlet temperature with feed interstitial velocity through the shell side of hollow fiber module at various inlet temperatures (MXFR #3; Feed: 1 % NaCl; distillate: deionized water at 15-17 °C, 1660 cm/min of linear velocity)

Interstitial velocity, cm/min	Feed inlet temperature, °C			
	60	70	80	85
	Feed outlet temperature, °C			
46	52.6	60	68.1	71.4
92	54.9	63.7	72.4	76.2
172	56.9	66.2	75.2	79.7
229	57.3	66.9	76.1	80.3

Table A10. Experimental data used in Figures 19. DCMD: Variation of water vapor flux with inlet temperature of hot brine (1% NaCl) as feed flowing through the shell side (cross flow) at various interstitial velocities (Module MXFR #3; tube side: 15-17 °C deionized water, linear velocity 1660 cm/min)

Interstitial velocity (cm/min)	Feed inlet temperature, °C				
	60	70	80	85	90
	Water vapor flux, kg/m^2-h				
400	13.5	19.3	24.9	30.3	
800	17.4	25.2	36.2	43.2	
1500	20.5	28.2	43.4	56.5	
2000	22	33.7	47.6	68.8	78.6

Table A11. Experimental data used in Figure 20. DCMD: Variation of water vapor flux and distillate outlet temperature with linear velocity of distillate (D.I. water) flowing through the tube side at entrance temperature of 15-23 °C (Module MXFR #3; shell side: brine solution (1% NaCl) at 85 °C, average interstitial velocity 229 cm/min)

Linear velocity, cm/min	Water vapor flux, kg/m^2-h	Distillate outlet temperature, °C
988	46.7	65.9
988	47.1	65.5
1625	49.7	51.3
2632	57.2	42.6
3899	62.3	35.5

Table A12. Experimental data used in Figure 21. DCMD: Variation of water vapor flux with interstitial velocity of hot brine (1% NaCl) as feed flowing through the shell side (cross flow) at various temperatures (Module MXFR #9, tube side: 15-20 °C D.I. water, average linear velocity 1646 cm/min)

Interstitial velocity, cm/min	Feed inlet temperature, °C			
	60	70	80	85
	Water vapor flux, kg/m^2-h			
47	0.509	0.767	1.006	1.114
91	0.845	1.131	1.52	1.986
173	1.111	1.71	2.533	3.301
236	1.526	2.139	2.906	3.799
315	1.57	2.469	3.473	4.252

Table A13. Experimental data used in Figure 22. DCMD: Variation of water vapor flux with interstitial velocity of hot brine (1% NaCl) as feed flowing through the shell side (cross flow) at various temperatures (Module MXFR #10, tube side: D.I. water at 15-23 °C , average linear velocity 1643 cm/min)

Interstitial velocity, cm/min	Feed inlet temperature, °C			
	60	70	80	85
	Water vapor flux, kg/m^2-h			
47	0.31	0.716	1.008	1.248
95	0.767		1.658	1.91
98		1.239		
158		1.741	2.312	3.045
172	1.067			
236	1.189	1.991	2.943	3.638
315	1.345		3.242	3.987
319		2.244		

Table A14. Experimental data used in Figure 23. DCMD: Variation of water vapor permeation flux with operating time for hot brine (1% NaCl) recirculating through the shell side with a velocity of 234 cm/min at 85.5 °C, and cold distillate water recirculating through tube side at a velocity of 1625 cm/min at 16 °C (Module MXFR #3)

Operating time, hr	Water vapor flux, kg/m^2-h
0	68.8
2.5	71.3
8.5	71.5
14.5	69.1
23	54.8
26.5	66.9
29.5	65.5
35.5	52.9
42.5	52.5
47	61.3
52	62
56	62
56.5	56.7
67.5	54
72	62
73	62
80	60
84.5	50.3
90.5	54.7
93.5	55.4
96	55.5
103	54
107	54.7
109.5	54.7
112.5	52.9
115.5	54.8
118.5	54.6